The Cryosphere, 19, 6865–6886, 2025
https://doi.org/10.5194/tc-19-6865-2025

The Cryosphere Open Access EGU

Modelling ocean melt of ice mélange at Greenland's marine-terminating glaciers

Lokesh Jain, Donald A. Slater, and Peter Nienow

School of GeoSciences, University of Edinburgh, Edinburgh, UK

Correspondence: Lokesh Jain (lokesh.jain@ed.ac.uk)

Received: 20 December 2024 – Discussion started: 23 January 2025
Revised: 4 September 2025 – Accepted: 28 September 2025 – Published: 18 December 2025

Abstract. Many of Greenland's marine-terminating glaciers have retreated and accelerated in recent decades, contributing significantly to sea level rise. Increased submarine melting of calving fronts is often cited as the dominant driver of this retreat. However, the presence of ice mélange and its associated buttressing force on a glacier terminus is also thought to significantly impact glacier advance and retreat. The buttressing force depends on the mélange thickness, and thickness will be modulated by ocean melt rate, but our understanding of the melting of ice mélange by the ocean remains limited, and it is not yet known how these melt rates vary across a range of glacial and environmental conditions. Here, we perform high-resolution numerical simulations using MITgcm to model the circulation of ocean waters through an ice mélange close to marine-terminating glaciers and estimate the resultant melt. We find that near-surface waters within the ice mélange always warm due to the upwelling of deep warm waters, driven both by the subglacial discharge plume and by the melt-driven convection at the sides of the icebergs themselves. We explore the sensitivity of mélange melt rate to environmental conditions, finding that melt rate increases sublinearly with subglacial discharge and supralinearly with ocean temperature. In this sense, mélange melt rate appears to respond to environmental forcing in a similar manner to submarine melting of the calving front, and can be parameterised as such. The magnitude of the simulated mélange melt rates ranges from 0.26 to 0.92 $\mathrm{m\,d^{-1}}$, which is in good agreement with observational estimates. This work is a step towards both a better understanding of ice mélange dynamics and a better parameterisation of its effects on glaciers and the ocean.

1 Introduction

Many of Greenland's marine-terminating glaciers have retreated (Catania et al., 2018; King et al., 2020) and accelerated (Howat et al., 2005; Joughin et al., 2012) in recent decades, contributing 10.8 ± 0.9 mm to sea level rise between 1992 and 2018 (The IMBIE Team, 2020). Understanding the interaction between the ice sheet and the ocean is key to explaining this behaviour. An increase in ocean temperatures due to a heightened influx of Atlantic water (Wood et al., 2021) is often cited as the dominant driver of glacier retreat, as warmer oceans lead to enhanced glacier submarine melting (Straneo and Heimbach, 2013) as well as increased iceberg calving (O'Leary and Christoffersen, 2013). However, recent work has shown that atmospheric warming can be just as significant an influence on submarine melting (Slater and Straneo, 2022): surface meltwater injected at depth into the ocean as subglacial discharge drives buoyant plumes which increase the turbulent transfer of heat from the ocean to the ice (Holland and Jenkins, 1999; Jenkins, 2011; Carroll et al., 2015). Whilst both oceanic and atmospheric forcing are important factors underpinning the behaviour of Greenland's glaciers, there is a third component which can have a substantial effect on the cycles of glacial advance and retreat: the presence or absence of ice mélange.

Ice mélange is a mixture of icebergs, bergy bits and sea ice which can be found in front of some tidewater glaciers (Straneo et al., 2016) and forms when the combination of ocean currents and surface winds are unable to remove icebergs from a fjord sufficiently quickly (Burton et al., 2018). As a result, a fjord with constrictions and a glacier with a high calving rate are more likely to have ice mélange. For some Greenlandic glaciers, ice mélange forms sporadically

when temperatures are low enough for thick sea ice to form, locking the icebergs in place (Burton et al., 2018), such as in the Uummannaq district of West Greenland (Howat et al., 2010). However, larger glaciers may have ice mélange which persists year round: this is the case for glaciers such as Sermeq Kujalleq (Jakobshavn Isbræ) (Amundson et al., 2010) and Helheim (Wehrlé et al., 2023). Nevertheless, the colder winter temperatures and sea ice growth which comes with it may serve to strengthen this permanent mélange (Robel, 2017). Indeed, as a granular material, the rheology of ice mélange changes seasonally due to the thickening and thinning of sea ice with changing temperatures (Amundson et al., 2010).

The presence of an ice mélange can have several impacts on a glacier and its fjord. Firstly, if coherent enough, it may exert a buttressing force onto the glacier terminus, typically transmitting stresses from the fjord walls backwards (Burton et al., 2018). This buttressing force increases with mélange thickness – a thicker mélange transmits more stress and is more resistant to stress-induced breaking (Robel, 2017). If the average force per unit width transmitted to the glacier terminus is sufficiently high (typically around $10^7\,\mathrm{N\,m^{-1}}$), this buttressing effect can cause calving to cease (Robel, 2017). If an ice mélange subsequently melts, it will thin and weaken, reducing the backstress provided by the mélange onto the glacier. This means calving is more likely to occur, initiating glacier retreat (Bevan et al., 2019). Indeed, the numerical modelling of Krug et al. (2015) suggests that ice mélange has a greater impact on the seasonal cycles of a glacier front than submarine melting, and observations of Sermeq Kujalleq by Joughin et al. (2020) suggest that the primary link between ice flow speed and ocean forcing is via mélange rigidity. Amundson et al. (2025) use a model of stress in proglacial mélange to show that the buttressing force depends on the basal mélange melt rate through an inverse power law relationship with an exponent of about -3, demonstrating the potential for small changes in ocean melt rate to have a large impact on the buttressing force.

Secondly, the melting of a mélange inputs a substantial flux of freshwater into the fjord. This meltwater flux can exceed that provided by subglacial discharge and submarine melting of the glacier terminus (Enderlin et al., 2016), and in one modelling study, iceberg melt was the largest annual freshwater source in the Helheim Glacier – Sermilik Fjord system (Moon et al., 2018). The cooling and freshening triggered by this submarine iceberg melting is generally localised in the upper water column, with the polar water located at intermediate depths typically warming due to iceberg melt-induced upwelling of warm Atlantic water (Davison et al., 2022). Moreover, the mélange meltwater flux may even deepen the neutral buoyancy depth of the subglacial plume (Kajanto et al., 2023). This not only lowers the depth at which the glacially-modified waters are exported downfjord, but also suppresses plume-driven glacier melting in the upper layer of the water column, thereby potentially promoting undercutting of the calving front. It is the impact of mélange melting which is the subject of this paper.

Observational estimates of the ocean melt rate of ice mélange are limited but the magnitudes obtained support the idea of mélange melt being a significant term determining mélange thickness. Enderlin et al. (2016) used remote sensing methods at Ilulissat Isfjord and Sermilik Fjord to estimate a melt rate of approximately $0.1–0.8\,\mathrm{m\,d^{-1}}$. Other observations of iceberg meltwater flux in Sermilik Fjord have demonstrated a strong seasonal signal peaking across August and September (Moyer et al., 2019b), whilst observations of the seasonal ice tongue at the glacier Kangiata Nunaata Sermia suggest an estimated melt rate of approximately $1\,\mathrm{m\,d^{-1}}$ (Moyer et al., 2017, 2019a).

With regards to modelling the ocean melt of ice mélange, studies have typically focused on how the meltwater flux from icebergs influences the large-scale fjord circulation and dynamics (Davison et al., 2020, 2022; Kajanto et al., 2023), with results indicating that the freshwater released by the melting of an ice mélange can drive a fjord-wide circulation which increases the net up-fjord heat flux (Davison et al., 2020). Such studies examining the fjord-scale impact of iceberg melting typically use the "IceBerg" package (Davison et al., 2020) as implemented in the ocean modelling software MITgcm to approximate iceberg melting. By assigning an iceberg concentration to each grid box and estimating the resultant melting by using the velocity-dependent three equation formulation (Jenkins, 2011), the IceBerg package freshens, cools and decelerates the ocean water in that grid box accordingly. However, this coarse approximation of the iceberg-melting process, necessary to run fjord-scale simulations (with a typical horizontal resolution of 300–500 m) in a reasonable computational time, is unable to resolve accurately how water flows between individual icebergs. One of the key tenets of the three equation formulation is that the melting of ice by the ocean depends on the velocity of the ocean; and since these studies do not resolve the velocity of the ocean around icebergs in high resolution, they are unable to analyse in detail the flow and thermodynamics related to ocean-induced melting of ice mélange, resulting in uncertainty in their melt rate estimates.

Hughes (2022) modelled ocean flow through an ice mélange at 10 m horizontal resolution, and was therefore able to resolve the ocean velocity in greater detail. He found that the presence of cuboid icebergs slows the flow in some places, particularly near the surface, but accelerates it in others, with the fastest current speeds being located at or below the drafts of the deepest icebergs. However, that study only examined the effect of the physical presence of an ice mélange on the flow through a fjord without including the effect of any melting processes. The melt rate of ice depends on the water velocity (Holland and Jenkins, 1999), such that variations in the magnitude and direction of water with respect to iceberg faces can influence their rate of melt (Fitz-Maurice et al., 2017; Hester et al., 2021). Therefore, it is

likely that the distribution of icebergs within mélange influences water velocity and iceberg melt rate.

Understanding in detail what factors are key in determining mélange melt rates is crucial to justifying the assumptions made in the IceBerg package and updating the parameterisations used in fjord-scale representations of iceberg melting. Hughes (2024) modelled the melting of icebergs in an ice mélange, including thermodynamic processes, and found melt rates of 0.3–0.4 m d^{-1}. This melt induces a flow of order 5 cm s^{-1}, and the fastest flows occur in localised hotspots near the surface where water is squeezed through the gaps between icebergs. However, a systematic analysis of the factors affecting the melt rate of an ice mélange has not yet been undertaken.

High resolution mélange melting simulations are therefore required to understand the fundamental processes behind the melting of ice mélange. In particular, it is important to gain a deeper understanding of how mélange melting varies under different glacial and environmental conditions – how sensitive are mélange melt rates to ocean temperatures, subglacial discharge flux, or the geometry of the mélange itself? Here, we model the melting of an artificially-created ice mélange using MITgcm to examine the sensitivity of the ocean melt rate of ice mélange (hereafter referred to as the mélange melt rate) to changes in glacial and environmental conditions. This paper proceeds as follows. Section 2 describes the methods, including the model setup, boundary conditions, and simulation details. Section 3 presents the results of our simulations. Section 4 discusses the implications of our findings, and Sect. 5 concludes the study and considers future research directions.

2 Methods

2.1 Model setup

We model the melting of an ice mélange using a model domain of 15 km × 5 km × 500 m (600 × 250 × 50 grid points) using the three-dimensional, non-hydrostatic ocean model MITgcm (Marshall et al., 1997a, b) at 20 m horizontal and 10 m vertical resolution within the mélange (Fig. 1a). The ice mélange itself has dimensions of 10 km × 5 km. The size of the domain and of the ice mélange has been chosen based on the Helheim Glacier – Sermilik Fjord system but is intended to be representative of large Greenlandic glacier-fjord systems. Working from west to east, the first layer of grid cells x_1 represents the calving front of a glacier. This layer is, therefore, made up entirely of ice cells, apart from a central 200 m × 30 m channel where subglacial discharge emerges. The second layer x_2 is open water; the layers x_j for $3 \leq j \leq 502$ are made up of an artificially-created ice mélange consisting of cuboid icebergs of a range of different shapes and sizes (see Sect. 2.3 for more details). The eastern-most 5 km of the domain, layers x_k for $503 \leq k \leq 600$, is a restoring region, consisting of open water and a sponge layer to allow the fluid flow to relax to the boundary conditions before exiting the domain. The resolution of this restoring region gradually decreases away from the mélange. The Coriolis parameter is set for 70° N ($f = 1.37 \times 10^{-4}$ s^{-1}).

2.2 Initial and boundary conditions

On the western side of the domain, fresh subglacial discharge emerges from beneath the glacier at a flux Q_0 at the pressure melting point (approximately −0.4 °C at a depth of 500 m; Fig. 1a).

The eastern boundary temperature T_0 and salinity S_0 profiles (Fig. 1b) are set by CTD profiles collected from near the end of the mélange in Sermilik Fjord, southeast Greenland (Straneo et al., 2011). These profiles demonstrate the presence of a warm, deep and salty Atlantic water layer in the bottom 400 m of the fjord, with a cooler and fresher surface layer above this in the upper 100 m. The salinity profile is kept constant for all runs, but in order to test the sensitivity of mélange melt to fjord temperature, we also generate anomalous positive and negative temperature profiles $T_{\pm\gamma}$ via

$$T_{\pm\gamma}(z) = T_0(z) \pm \frac{\gamma}{2}\left[\tanh\left(\frac{z-100}{30}\right)+1\right] \quad (1)$$

where $\gamma = 1.0$ or 2.0 °C is the magnitude of the desired temperature anomaly; z is the (positive) depth below the surface; 100 m is the target depth at which the anomalous temperature profile should start diverging from the baseline temperature profile; and 30 m is the approximate height of the layer over which the temperature profile changes from the baseline profile to the anomalous profile (Fig. 1b). We set a depth at which the temperature profile should start diverging as we do not wish to change the initial temperature of the surface waters between simulations. The reason for this is that we expect water near the surface will be very strongly affected by the melting of the ice mélange, whereas water at depth is upwelled by the plume. We therefore vary the temperature of these deeper waters which are the source of the heat which drives the melting of the ice mélange.

The initial conditions of a particular simulation are set to be the same as the boundary conditions. However, because the simulations are run until they have reached approximate steady state (Sect. 2.6), we note that the model is insensitive to this initialisation; the simulations are run for long enough that the model effectively forgets the initial conditions. The final state which the model evolves to is dependent only on the boundary conditions and the fixed mélange geometry.

2.3 Making a mélange

In order to investigate systematically how mélange geometry affects the melting of mélange, we sought a way to generate an artificial mélange whose properties we could then vary between simulations. The icebergs which constitute this

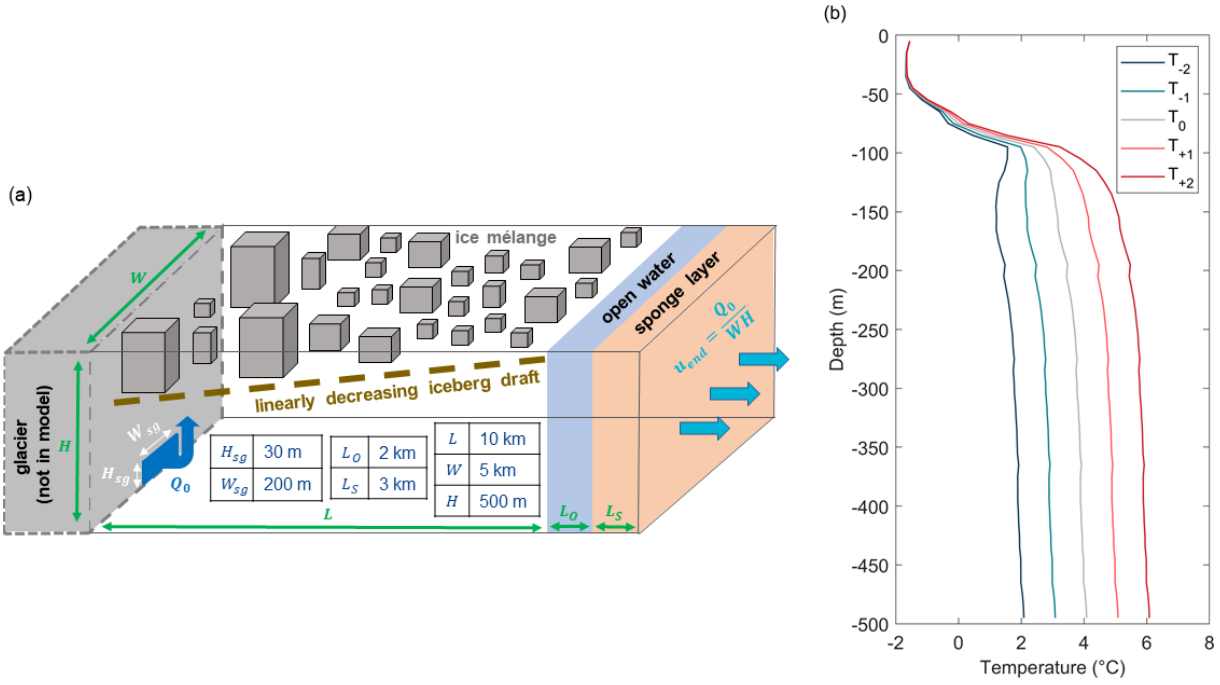

Figure 1. (a) A schematic of the model set up. The fjord is 15 km × 5 km × 500 m. The ice mélange (10 km × 5 km) has a linearly decreasing draft away from the glacier terminus and is represented by cuboid icebergs using the MITgcm packages ShelfIce and IceFront. Subglacial discharge Q_0 emerges from beneath the calving front from a channel of size $H_{sg} \times W_{sg}$. A sponge layer is implemented on the eastern side of the domain to gradually relax the fluid flow to ambient conditions before exiting the domain. **(b)** The various temperature profiles used in this study. A standard temperature profile T_0 is taken from observations from Sermilik Fjord (Straneo et al., 2011); the other profiles are generated according to Eq. (1).

artificial mélange had to have certain realistic characteristics. Firstly, the artificial icebergs had to replicate observed iceberg size power law distributions $N \propto A^{-\alpha}$, where N is the number of icebergs of horizontal surface area A (Sulak et al., 2017; Åström et al., 2021; Shiggins et al., 2023). Secondly, the artificial icebergs had to have realistic aspect ratios such that the volume V of an iceberg is related to its area A by $V = aA^b$, with the 95 % confidence interval for a and b being $3.4 < a < 8.6$ and $1.26 < b < 1.33$ (Sulak et al., 2017). Thirdly, the artificial icebergs had to have a mean draft which varied down-fjord in agreement with observations of mélange thickness (Enderlin et al., 2016; Meng et al., 2024).

In order to respect all of these constraints, we randomly sample icebergs from the following power law distribution for the number of icebergs N of draft H (see Appendix A for more details):

$$N(H) = \left(\frac{1-\beta}{H_{\max}^{1-\beta} - H_{\min}^{1-\beta}} \right) H^{-\beta} \tag{2}$$

where $H_{\min}$ and $H_{\max}$ are the smallest and largest iceberg draft in the distribution, and β varies with distance away from the glacier terminus. Equation (2) has been derived assuming the aforementioned iceberg size power law distribution and realistic aspect ratios, and the value of β is determined based on observations of mélange thickness.

We randomly sample icebergs from the distribution using inverse transform sampling (Appendix B) until the iceberg areal fraction λ (i.e. the percentage areal coverage of the fjord surface covered by icebergs) reaches a desired value. For the majority of the simulations, we set $\lambda = 0.6$, which represents a very densely packed ice mélange. There are limited estimates of λ within a mélange: Foga et al. (2014) use satellite remote sensing techniques at Helheim Glacier to determine an iceberg-to-sea ice ratio of between 0.0 and 0.35; assuming a mélange is made up entirely of icebergs and sea ice, this corresponds to $0.0 \leq \lambda \leq 0.26$. Sulak et al. (2017) classify up to 39 % of the total ice area in an ice mélange as icebergs, corresponding to a maximum value of $\lambda = 0.39$. In light of these smaller estimates of λ, we run six additional simulations with $0.2 \leq \lambda \leq 0.5$ as a sensitivity test (precise details in Sect. 2.6 and Table C).

Once enough icebergs have been sampled such that λ has been reached, these artificial icebergs are then placed into the domain within MITgcm via the ShelfIce package (Losch, 2008). The icebergs both inhibit the flow of water and generate freshwater via melting (Sect. 2.4). In light of each simulation run time (Sect. 2.6) and the modelled melt rates (Sect. 3.1.2), changes in iceberg geometry over time are less than the model resolution and are thus ignored in our simulations.

The standard mélange profile used in the simulations (Fig. 2a) has a mean iceberg draft of 100 m at the calving front and 50 m at a distance of 10 km down-fjord, motivated by observations of the ice mélange in Sermilik fjord (Enderlin et al., 2016). There is much variability in the sizes of icebergs everywhere in the domain, as is to be expected – large icebergs occasionally travel a long way down-fjord, and small icebergs are also found very close to the glacier terminus. Whilst the icebergs generated in this segment follow the underlying target probability distribution quite closely (Fig. 2b), the icebergs actually placed in the mélange diverge from this slightly. If the domain were an infinite size then this would not be a problem; however, trying to squeeze all of the generated icebergs into a finite space whilst also ensuring $\lambda = 0.6$ means that some deviation is likely to occur.

In addition to the standard mélange profile, we also run simulations with a thick mélange profile and a thin mélange profile. We do this to investigate the effect that the thickness of a mélange has on the simulated melt rate of the icebergs in the mélange. The thickness of the artificial mélange is adjusted by varying the parameter β accordingly in Eq. (2) (Appendix A). The thick (thin) profile has a mean draft of 200 m (50 m) at the calving front and 100 m (25 m) at a distance of 10 km down-fjord. These values are chosen based on the range of observed mélange thicknesses at both Helheim Glacier and Sermeq Kujalleq (Enderlin et al., 2016; Meng et al., 2024). The mean thickness profile for all mélange configurations is very close to the target mean draft (Fig. 2c). For a given value of λ, the thin mélange profile will have more icebergs than the thick mélange profile.

Our simulated mélange submerged area (for an iceberg areal fraction of $\lambda = 0.6$) ranges from 65 km^2 (thick mélange) to 92 km^2 (thin mélange). This is slightly lower than the observations of Enderlin et al. (2016), who estimate that the area varies from 132–261 km^2. However, we note that Enderlin et al. (2016) include growlers, bergy bits and sea ice in their mélange area estimates, which likely accounts for our lower values of the mélange submerged area. The lowest mélange submerged area in this study is the $\lambda = 0.2$ simulation, with an area of only 29 km^2.

Note that the mélange we generate here does not include sea ice. This is because we do not expect sea ice to contribute significantly to the mélange meltwater flux – as a thin layer near the surface, the water surrounding sea ice is predominantly cool and stagnant, and so we do not expect sea ice to melt significantly compared to the icebergs in a mélange.

2.4 Representation of melting

We represent iceberg melting using the typical three-equation melt parameterisation (Holland and Jenkins, 1999; Jenkins, 2011) which ensures that, at the ice-ocean interface: (a) heat flux through the ice-ocean boundary layer is balanced, (b) salt flux through the ice-ocean boundary layer is balanced, and (c) the temperature of the ice-ocean boundary layer is at the pressure melting point. However, this parameterisation relies on a number of constants whose values are plagued with uncertainty (Zhao et al., 2024).

One such constant is the drag coefficient, C_d. In the three-equation melt parameterisation, the heat flux to the ice is strongly controlled by the drag coefficient, with the melt rate of the ice $m \propto \sqrt{C_\mathrm{d}}$, and so an accurate representation of drag in a model is crucial in order to simulate melt rates realistically. A value of $C_\mathrm{d} = 2.5 \times 10^{-3}$ is typically used (Jenkins et al., 2010). However, some studies have found that using this value of the drag coefficient underestimates melt rates at glacier faces (Sutherland et al., 2019; Jackson et al., 2020). Moreover, as Zhao et al. (2024) argue, using a single value for the drag coefficient does not distinguish between a range of possible flow scenarios at the ice-ocean interface along the face of an iceberg. The heat flux to the ice will likely depend on whether the interface is horizontal or vertical. The heat flux to the ice will also depend on whether the fluid flow is primarily driven by plume-driven convection, melt-driven convection, or a general fjord-wide horizontal flow and overturning circulation (Zhao et al., 2024). It is therefore important to adjust the value of C_d in the melt rate parameterisation according to the fluid flow in a particular grid cell in order to accurately represent iceberg melting in MITgcm.

The current three-equation melt parameterisation could be improved by incorporating the interface slope and driver of the fluid flow directly into the determination of the ice melt rate. However, as a temporary solution, we suggest that the modelled velocity itself can be used as an effective mask that identifies different regimes of melting. In particular, modelled regions undergiong melt-driven convection have ice-adjacent velocities less than $0.04\,\mathrm{m\,s^{-1}}$, and the only place in the simulations where fluid velocities are greater than $1\,\mathrm{m\,s^{-1}}$ is in the plume itself. We therefore assign values of the drag coefficient based on Zhao et al. (2024) and the modelled ice-adjacent velocity in a particular grid cell:

1. Melt-driven convection: $|u| \leq 0.04\,\mathrm{m\,s^{-1}}$, $C_\mathrm{d} = 0.15$
2. Horizontal flow: $0.04\,\mathrm{m\,s^{-1}} < |u| \leq 1.00\,\mathrm{m\,s^{-1}}$, $C_\mathrm{d} = 0.0025$
3. Plume-driven convection: $|u| > 1.00\,\mathrm{m\,s^{-1}}$, $C_\mathrm{d} = 0.015$

where $|u|$ is the velocity magnitude accounting for both horizontal and vertical components. We impose a minimum background velocity of $0.04\,\mathrm{m\,s^{-1}}$ at each lateral iceberg face to represent unresolved melt-driven convection (Cowton et al., 2015). In practice, what this means is that we assume melt-driven convection occurs everywhere; if the velocity of fluid at the ice-ocean interface is calculated to be above $0.04\,\mathrm{m\,s^{-1}}$, then we enter the horizontal flow regime; and if the velocity of the fluid is above $1\,\mathrm{m\,s^{-1}}$, then we enter the plume-driven convection regime.

Whilst this method has the disadvantage of not being very elegant (an all-encompassing melt rate parameterisa-

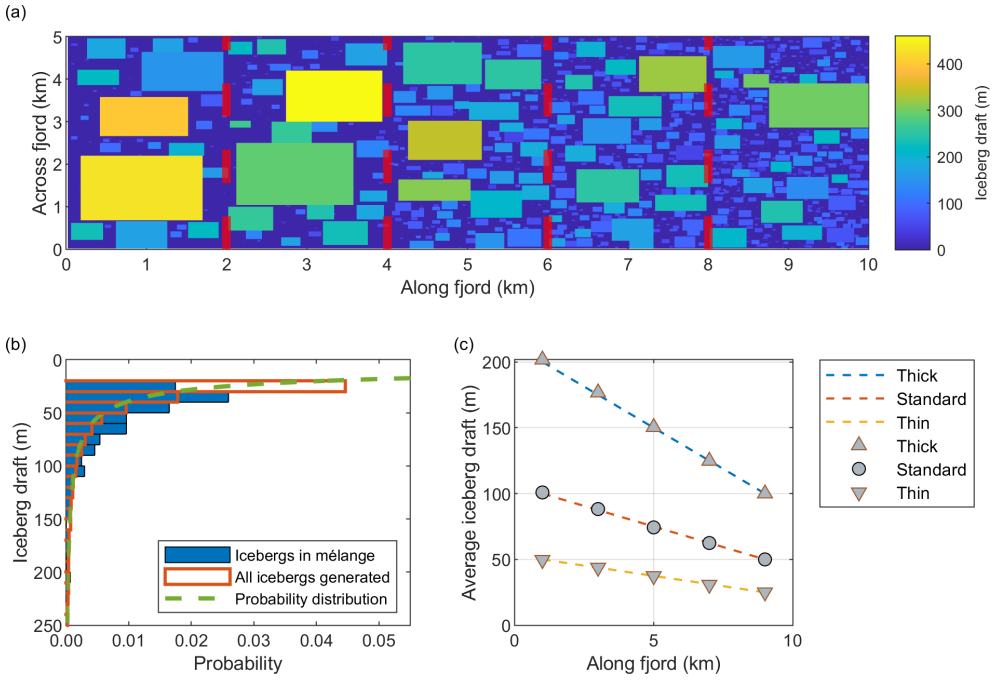

Figure 2. (a) A plan view of the standard mélange profile used in the simulations. The mélange is split into five segments (delineated by the dashed red lines) each with a length along fjord of 2 km. Each segment has a distinct mean iceberg draft; this mean average draft decreases down fjord to represent the thinning of a mélange. **(b)** The distribution of icebergs in the final segment with a mean iceberg draft of 50 m. In orange are all the icebergs generated; in blue are all the icebergs actually placed in the mélange. Not all generated icebergs are placed because icebergs stop being placed once the iceberg areal fraction $\lambda = 0.6$. In green is the underlying probability distribution from which the icebergs are generated. **(c)** The mélange profiles target mean draft (dashed line) and actual mean draft (markers) for the thick, standard and thin profiles.

tion would be more rigorous), it has the advantage of being consistent both with Zhao et al. (2024) and also with other literature suggesting that the standard value of $C_d = 2.5 \times 10^{-3}$ underestimates the melt rate at the ice-ocean interface (Sutherland et al., 2019; Jackson et al., 2020).

We represent melting in MITgcm using the ShelfIce (Losch, 2008) and IceFront (Xu et al., 2012) packages for basal and lateral melting respectively. With respect to the other constants in the three-equation melt parameterisation, we set the turbulent transfer coefficients of heat and salinity to $\Gamma_T = 2.2 \times 10^{-2}$ and $\Gamma_S = 6.2 \times 10^{-4}$ respectively (Jenkins, 2011).

2.5 Introduction of key analysed quantities

We analyse the simulations in terms of the modelled circulation, the modelled temperature, the mean mélange melt rate and the total mélange meltwater flux. The latter two deserve a specific definition since their calculation must take account of the geometry of the mélange. For each ocean grid cell i, we calculate the total meltwater flux ϕ_i into that grid cell as $\phi_i = m_{i,s}A_{i,s} + m_{i,b}A_{i,b}$ where $m_{i,s}$ [$m_{i,b}$] and $A_{i,s}$ [$A_{i,b}$] are the melt rate and area of ice on the sides [bottom] of icebergs available for melting in grid cell i. We then define the mean melt rate m_i in grid cell i as $m_i = \phi_i / A_i$ where $A_i = A_{i,s} + A_{i,b}$ is the total area of ice available for melting in a given grid cell.

The total mélange meltwater flux is then defined as $\Phi = \sum_i \phi_i$ and the mean mélange melt rate is defined as $m = \sum_i m_i / N$ where N is the number of ocean grid cells in contact with ice. Since we wish to focus on melting of the ice mélange, melting of the calving front is included in the simulations but is not included in our analysed quantities.

2.6 Simulations run

We vary the subglacial discharge flux Q_0, the temperature profile of the fjord, the mélange thickness profile and the iceberg areal fraction between simulations and we analyse the subsequent impact on mélange melt rates. We test the sensitivity to subglacial discharge by applying values of $0, 10, 30, 100, 300, 600$ and $1000\,m^3\,s^{-1}$ in simulations that use the standard temperature profile, standard mélange thickness and iceberg areal fraction $\lambda = 0.6$ (totalling 7 simulations). These subglacial discharge values are similar to those observed and modelled at a large Greenlandic glacier such as Helheim throughout the year (Mankoff et al., 2020; Karlsson et al., 2023).

We test the sensitivity to the temperature profile by running simulations with the two colder profiles and two warmer

profiles assuming a standard mélange thickness, $\lambda = 0.6$, and with subglacial discharge values of 10, 300 and 1000 $m^3 s^{-1}$ (totalling 12 simulations). We test the sensitivity to mélange thickness by running simulations with the thin and thick mélange assuming the standard temperature profile, $\lambda = 0.6$, and (again) with subglacial discharge values of 10, 300 amd 1000 $m^3 s^{-1}$ (totalling 6 simulations). Lastly, we test the sensitivity to the iceberg areal fraction λ by running simulations with $\lambda = 0.2, 0.3, 0.4, 0.5$ assuming the standard mélange thickness, standard temperature profile and $Q_0 = 300$ $m^3 s^{-1}$; a final two simulations have $\lambda = 0.2$ with the standard mélange thickness, standard temperature profile and $Q_0 = 10, 1000\,m^3\,s^{-1}$ (totalling 6 simulations). The final set of 31 simulations (shown in Table C1 in Appendix C) thus does not consider every possible permutation of choices but is a manageable and representable set to investigate what controls ice mélange melt.

The simulations are run until they have reached an approximate steady state, which we define as when both the (a) water temperature and salinity and (b) mélange melt rate and meltwater flux do not vary significantly from one timestep to another. Most simulations reach steady state after approximately six days of simulation time. The results throughout Sect. 3 are averages taken whilst the model is in steady state, typically over the last 17 h of a model run.

3 Results

Results are presented as follows: in Sect. 3.1, we show the qualitative features of a representative simulation (specifically, the standard mélange thickness, $Q_0 = 300\,m^3\,s^{-1}$ and T_0 temperature profile simulation ms_q300_t0 as specified in Table C1). In Sect. 3.2, we consider all simulations, covering the sensitivity of mélange melting to subglacial discharge, fjord temperature and mélange thickness, before attempting to find a parameterisation that captures these dynamics.

3.1 Single simulation

3.1.1 Circulation and properties

The influx of subglacial discharge and the resultant buoyant plume sets up a general overturning circulation in the middle of the fjord, with down-fjord flow in the upper 200 m of the domain and an up-fjord flow layer beneath this (Fig. 3a). This down-fjord flow is fastest in the first couple of kilometres downstream from the glacier front. The water flow driven by the subglacial discharge is highly disrupted by the presence of an ice mélange (Fig. 3b). In particular, the horizontal flows have to find open pathways through the icebergs in order to travel down-fjord, and this results in acceleration of the flow in some places as the water is squeezed between icebergs, and deceleration of the flow in other places. The specific pathways of fastest water flow are highly dependent on the specific configuration of each ice mélange.

The subglacial discharge plume upwells warmer waters from depth into the upper water column in the first 2 km of the domain (Fig. 3c). The mélange acts as a heat sink for the plume: as the plume advances down-fjord, the mélange extracts heat from it for melting until all of the heat is lost. Note that the warm water in the first 2 km of the domain (Fig. 3c) is not a transient feature whereby a pulse of warm water is gradually moving down-fjord; it is a steady state feature. Further along, the temperature profile in the middle of the fjord is remarkably similar to the restoring temperature profile, with only pockets of warm water upwelling into the upper layers.

There is a general upwelling of water around icebergs seen as a "halo" surrounding each iceberg (Fig. 3d). This is due to melting on the sides of each iceberg forming little buoyant plumes of meltwater which rise up the iceberg face. As discussed in Sect. 2.4, this melt-driven convection is not fully resolved in the model and so is parameterised by imposing a minimum background velocity of 0.04 $m\,s^{-1}$ at each lateral iceberg face. Also visible is an alternating pattern of upward and downward velocities near (within ~ 1 km of) the subglacial discharge outlet – this is most likely a wave set up by the plume as it travels down-fjord and oscillates around its level of neutral buoyancy.

Averaging across the fjord and within the top 200 m of the water column, the velocity signal of the flow through the mélange fluctuates significantly due to the presence of icebergs (Fig. 4). The large variation in iceberg size and number in any given horizontal slice through the domain leads to much variability in ocean velocity as the flow navigates its way through the ice mélange. On top of this variability is a clear decreasing down-fjord trend in velocity (Fig. 4a) and a peak in the middle of the fjord where the subglacial discharge outlet is located (Fig. 4b). Both the water velocity and temperature are higher in the northern side of the fjord (Fig. 4b), which suggests that the subglacial discharge plume is primarily travelling along the northern edge of the domain. This is likely due to the specific configuration of icebergs in the mélange: in other configurations of icebergs this particular asymmetry disappears. The peak velocity depth is located at approximately 100 m below the surface (Fig. 4c). This corresponds to the depth at which the plume outflows down the fjord and is determined by both the level of neutral buoyancy of the plume and the density of icebergs in the mélange, since the plume needs to be able to navigate around icebergs efficiently to advance down-fjord.

The upwelling of warm water driven by the buoyant plume leads to a warming of up to 2 °C in the upper 100 m of the fjord (Fig. 4c). The temperature decreases down-fjord away from the glacier terminus (Fig. 4a) due to the mélange extracting energy from the plume for melting; as the available energy decreases, so therefore does the mean water temperature. There is also cooling with respect to the ambient conditions at mid-depth ($\sim$ 100–400 m) (Fig. 4c) due to iceberg melting and mixing of cooler surface waters downwards.

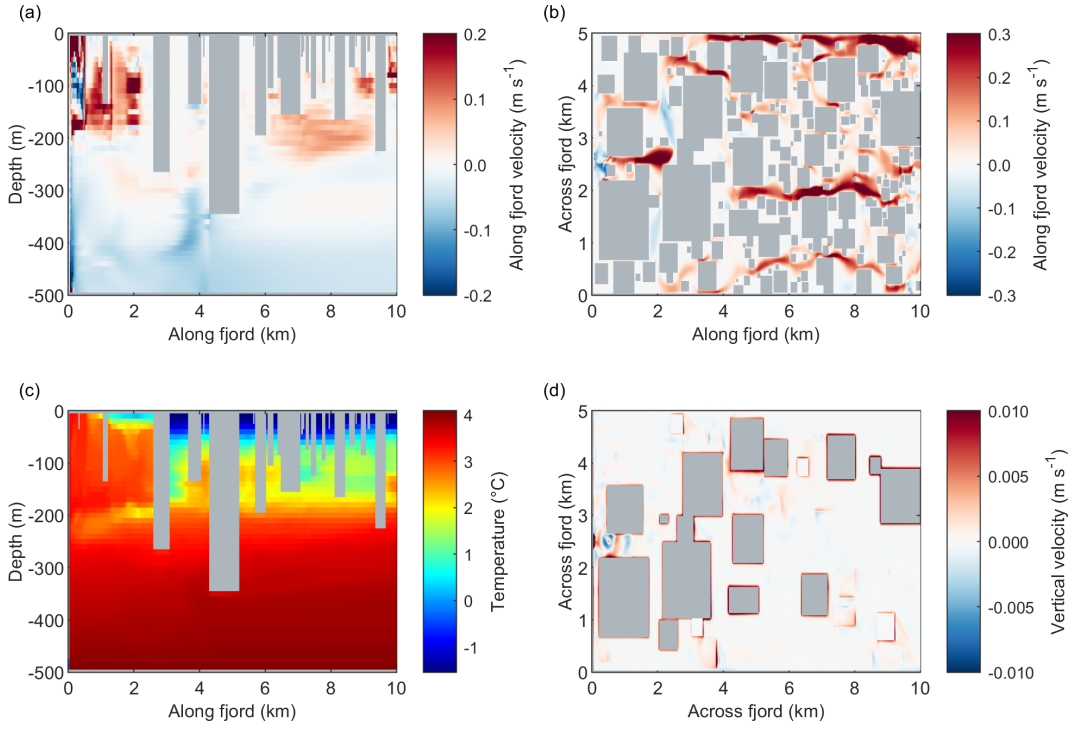

Figure 3. Along fjord and plan view plots of the mélange illustrating global circulation and temperature profile at the end of the model run. Icebergs within the mélange are shown as dark grey. The figures are generated by averaging over the last 17 h of the model run, whilst the model is in steady state. **(a)** An along fjord plot of along fjord velocity from the middle of the fjord at $y = 2.5$ km. **(b)** A plan view plot of along fjord velocity from a depth of 100 m. **(c)** An along fjord plot of temperature from the middle of the fjord at $y = 2.5$ km. **(d)** A plan view plot of vertical velocity at a depth of 250 m.

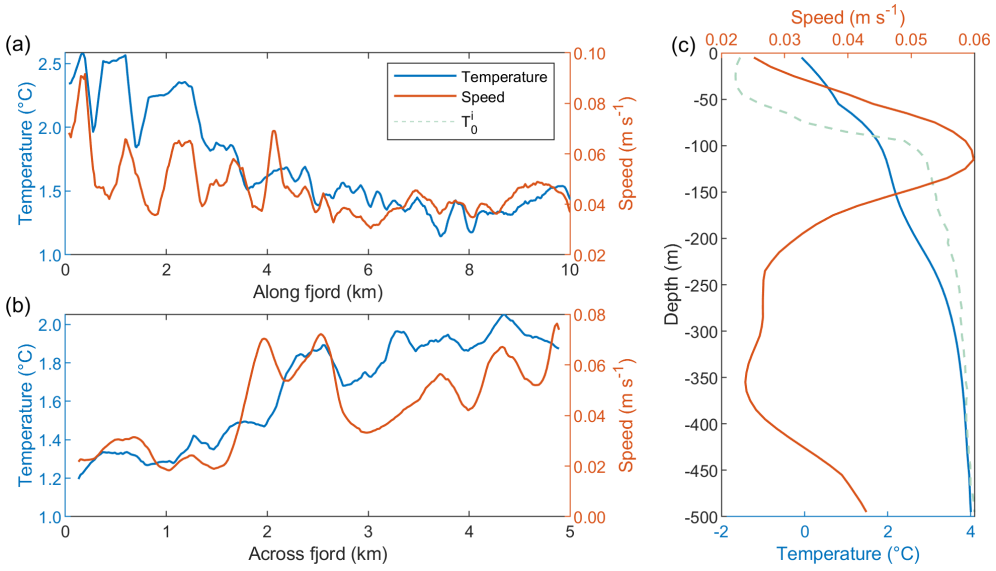

Figure 4. Along fjord **(a)**, across fjord **(b)** and depth **(c)** variation of temperature and flow speed throughout the mélange at the end of the model run. All variables are smoothed using a moving average with a window size of 10 grid cells, which is 200 m for the horizontal plots **(a)** and **(b)** and 100 m for the vertical plot **(c)**. The flow speed is $V = \sqrt{u^2 + v^2 + w^2}$ where u, v and w are the x, y and z components of the velocity respectively. The along fjord and across fjord plots are averaged over the upper 200 m of the fjord, which is the depth relevant to the melting of the ice mélange.

3.1.2 Melt rates and fluxes

The mélange melt rate decreases with distance down-fjord (Fig. 5a), due partly to decreasing ocean temperature and velocity (Fig. 4a), but also due to the fact that the mélange gets thinner with distance down-fjord and is therefore sitting in shallower, cooler waters. The depth at which melt rates are highest is approximately 400 m (Fig. 5c) due to a combination of high vertical velocity as a result of water upwelling from deep icebergs (Fig. 3d) and warm ocean temperatures at this depth (Fig. 4c). The melt rate is higher in the northern half of the domain (Fig. 5b), likely due to the water velocity and temperature being higher in this region (Fig. 4b). As noted previously, the subglacial discharge plume preferentially travels in this section of the fjord due to the particular configuration of icebergs present. The average melt rate across the entire mélange is $m = 0.59\,\mathrm{m\,d^{-1}}$.

There is a considerable fluctuation in the mélange meltwater flux due to a variation in iceberg size and number throughout the domain, but the flux decreases slightly with distance down-fjord (Fig. 5a). The meltwater flux is the sum of the melt rate multiplied by the surface area available for melting. Far away from the glacier terminus, low melt rates (Fig. 5a) combine with the high surface area of lots of small, shallow icebergs (Fig. 2) to maintain a similar meltwater flux to the region near the glacier terminus. The depth at which the meltwater flux is highest is approximately 100 m (Fig. 5c); despite melt rates being relatively low at this depth, the large area of ice available for melting results in the high meltwater flux. The total meltwater flux is $\Phi = 510\,\mathrm{m^3\,s^{-1}}$ and the total submerged surface area of ice available for melting is $A = 79\,\mathrm{km^2}$.

The melt rate and meltwater flux are spatially correlated across the fjord (Fig. 5b) but not along the fjord (Fig. 5a). This is because the primary variability in melt rate occurs along the fjord – further away from the terminus, decreasing ocean temperatures and velocity combined with a thinner mélange lead to lower melt rates, whilst a larger surface area of smaller icebergs mitigate the reduction in meltwater flux. However, in the across-fjord plot of Fig. 5b, this along-fjord variation is averaged over the full length of the mélange, allowing a second-order variation to come through. This second order variation in melt rate arises due to the position the plume takes through the mélange as well as the presence or absence of large, deep icebergs, both of which also directly impact the meltwater flux.

3.2 All simulations

In Sect. 3.2.1–3.2.3, the influence of varying the subglacial discharge, ambient ocean temperature and mélange thickness on the steady state water temperature, water velocity, mélange melt rate and mélange meltwater flux is discussed. In Sect. 3.2.5, the mean melt rate and total meltwater flux across all simulations is analysed, and a parameterisation for mélange melting is developed in Sect. 3.2.6.

3.2.1 Sensitivity to subglacial discharge

All simulations, irrespective of the magnitude of the subglacial discharge, show cooling with respect to the ambient temperature profile beneath a depth of 100 m and warming above this depth (Fig. 6a), similar to the single simulation discussed in Sect. 3.1.2 (Fig. 4c). However, above 150 m the temperature profiles diverge with higher subglacial discharge resulting in warmer ocean waters in the upper water column. This is because higher subglacial discharge generates a more vigorous plume, entraining more warm water from depth.

A higher subglacial discharge leads to a higher velocity magnitude above a depth of around 150 m (Fig. 6b). A larger subglacial discharge flux generates a stronger plume, which in turns sets up a stronger fjord-wide circulation. The depth of the peak velocity is likely a reflection of the neutral buoyancy depth of the outflowing plume: a higher subglacial discharge flux generates a fresher plume, which makes the neutral buoyancy depth more shallow. Thus, for $Q_0 = 10\,\mathrm{m^3\,s^{-1}}$, the level of neutral buoyancy is at a depth of 140 m, whereas for $Q_0 = 1000\,\mathrm{m^3\,s^{-1}}$ its depth is approximately 90 m.

Below a depth of 150 m, both the melt rate and the meltwater flux are insensitive to the magnitude of subglacial discharge (Fig. 6c). This suggests that the melting of deeper-drafted icebergs are unaffected by changes in subglacial discharge. In the upper 150 m, larger subglacial discharge leads to both higher melt rates and meltwater fluxes, due to a combination of higher temperatures and higher velocities here. The $Q_0 = 0\,\mathrm{m^3\,s^{-1}}$ and $Q_0 = 10\,\mathrm{m^3\,s^{-1}}$ simulations are remarkably similar, showing that the overall circulation set up by a very weak plume is comparable to the circulation in the complete absence of a plume. This demonstrates that the melting of the ice mélange alone is itself responsible for driving a weak circulation.

3.2.2 Sensitivity to ambient temperature

The basic shape of the temperature profile at the end of the model run is the same regardless of the temperature anomaly (Fig. 7a), with warmer deep waters resulting in mélange ocean temperatures that are warmer throughout the water column. The temperature differential between profiles decreases higher up the fjord, reflecting the shape of the ambient temperature profiles (Fig. 1b).

Higher temperatures lead to slightly higher velocities throughout the entire depth of the water column (Fig. 7b). This is because warmer ocean temperatures lead to more mélange melting, which in turn results in greater upwelling on the sides of icebergs in the mélange. This increase in upwelling (which reflects an increase in the rate of melt-driven convection) leads to a more vigorous fjord circulation. A

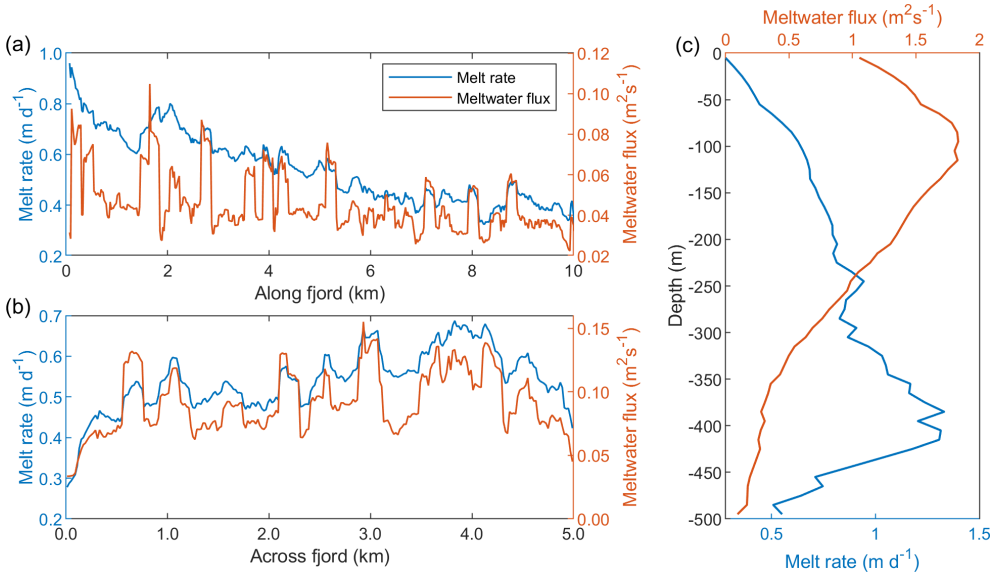

Figure 5. The average melt rate and total meltwater flux **(a)** along the fjord **(b)** across the fjord **(c)** with depth. The meltwater flux is given in units of $m^2\,s^{-1}$ (i.e. $m^3\,s^{-1}$ per unit distance), so that the total meltwater flux is the area under the curves. All variables are smoothed using a moving average with a window size of 10 grid cells, which is 200 m for the horizontal plots **(a)** and **(b)** and 100 m for the vertical plot **(c)**. The along fjord and across fjord plots are averaged over the upper 200 m of the fjord, which is the depth relevant to the melting of the ice mélange.

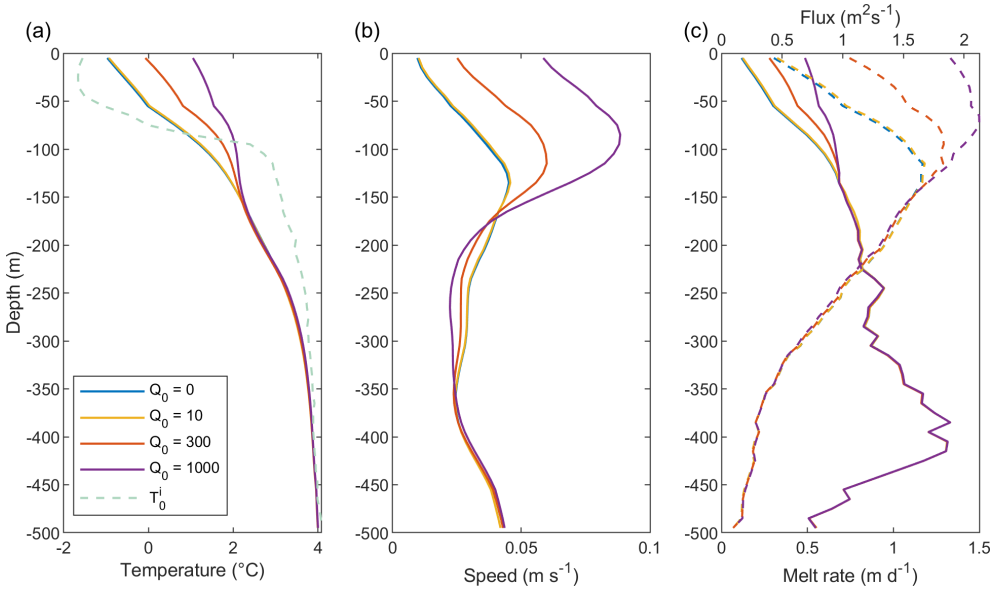

Figure 6. Sensitivity of ocean dynamics in the mélange to subglacial discharge flux. **(a)** Temperature. The dashed line shows the imposed boundary condition. **(b)** Flow speed and **(c)** mélange melt rate (solid) and meltwater flux (dashed). All simulations have a temperature profile T_0, shown as the dashed line in **(a)**, a standard mélange thickness, and an iceberg areal fraction $\lambda = 0.6$. All variables are averaged over the area of the mélange (the full width and depth of the fjord and 10 km down-fjord of the glacier terminus).

change in the ambient temperature of $\pm 2\,°C$ only leads to a change in the velocity magnitude of $\Delta V < 1\,cm\,s^{-1}$.

A higher restoring temperature profile leads to a higher melt rate and meltwater flux at all depths since there is more heat available for melting the mélange (Fig. 7c). The difference in the meltwater flux between simulations is smallest at depth (since there are very few icebergs melting at this depth so there is little area available for melting) and grows with increasing height (since there are more icebergs and so more area is available for melting).

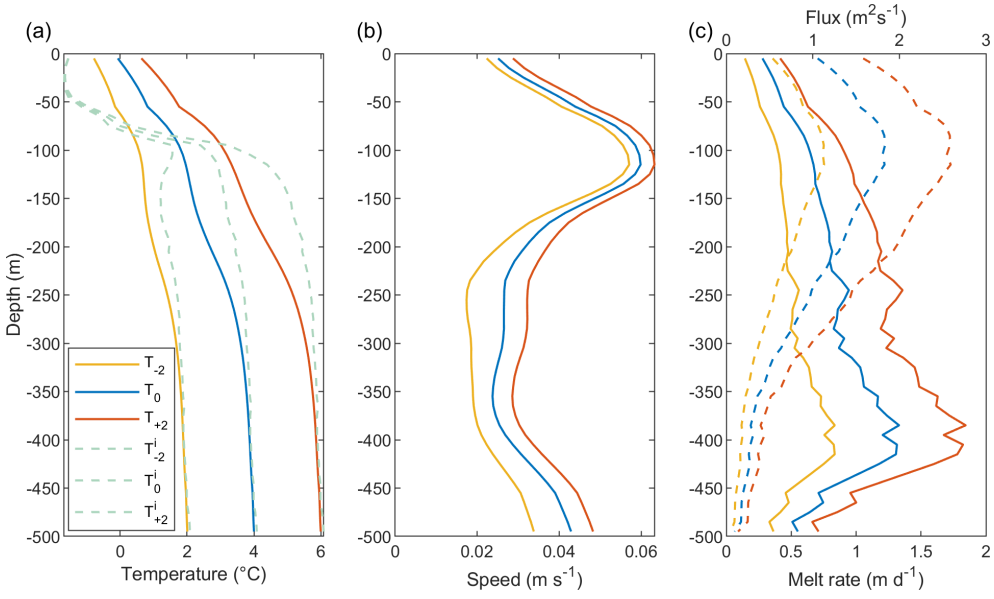

Figure 7. Sensitivity of ocean dynamics in the mélange to deep water temperature. **(a)** Temperature. The dashed lines show the imposed boundary conditions. **(b)** Flow speed and **(c)** mélange melt rate (solid) and meltwater flux (dashed). All simulations have a subglacial discharge flux $Q_0 = 300\,\mathrm{m^3\,s^{-1}}$, a standard mélange thickness and an iceberg areal fraction $\lambda = 0.6$. All variables are averaged over the area of the mélange (the full width and depth of the fjord and 10 km down-fjord of the glacier terminus).

3.2.3 Sensitivity to mélange thickness

A thicker mélange leads to more homogenisation of water temperature in the upper 200 m of the fjord and warmer near-surface waters (Fig. 8a). Both of these effects are due to increased upwelling from deeper icebergs with respect to the thinner mélange profiles. Similar to an enhanced subglacial meltwater flux and a warmer ambient ocean, a thicker mélange increases upwelling and generates a more vigorous circulation. Hence, each of these processes causes an increase in upper-layer velocities (Fig. 8b). The influence of mélange thickness on melt rates and meltwater fluxes is complex (Fig. 8c), but in general melt rates respond to changes in the modelled temperature and velocity, with a thicker mélange having a higher melt rate near the surface due to high water temperatures and velocities in this region. The meltwater flux peaks at a depth of approximately 100 m for a thin mélange, but this flux is more spread out and peaks at a lower depth for a thick mélange.

3.2.4 Sensitivity to iceberg areal fraction

Smaller iceberg areal fraction λ results in warmer temperatures throughout the water column (Fig. 9a). Fewer icebergs in the mélange generate a lower total meltwater flux, resulting in less cooling and therefore higher temperatures. Smaller λ also shallows the depth of peak flow speed (Fig. 9b) – a lower density of icebergs means that the plume is more likely to find a suitable path to advance down-fjord higher up in the water column. The simulation with $\lambda = 0.4$ has the lowest value for the maximum flow speed of approximately $0.05\,\mathrm{m\,s^{-1}}$, with both $\lambda = 0.2$ and $\lambda = 0.6$ reaching peak flow speeds of approximately $0.06\,\mathrm{m\,s^{-1}}$ (Fig. 9b). A low iceberg density may facilitate a fast shallow flow between the icebergs, whereas a high iceberg density may facilitate a relatively continuous flow along the bottom of the icebergs. In the upper 250 m of the water column, melt rates are similar regardless of λ, though there is a trend for slightly lower melt rates for higher λ (Fig. 9c). The main differences come at depth, where smaller λ is associated with fewer very deep icebergs and so deep melt rates can drop to zero. The iceberg meltwater flux generally increases with λ since larger λ results in more iceberg surface area (Fig. 9c).

3.2.5 Overall melt rates and fluxes

For given ocean boundary conditions and mélange thickness profiles, the sensitivity of overall mean mélange melt rate to subglacial discharge is sublinear in all cases (Fig. 10a). Melt rates increase sublinearly with subglacial discharge due to both the increased upwelling of warm waters (Fig. 6a) and more vigorous circulation (Fig. 6b). This sublinear dependence is due to the fact that the volume flux entrained by the plume scales sublinearly with subglacial discharge (Cowton et al., 2016). This is in contrast to the sensitivity of melt rates to deep water temperature, which is supralinear (i.e. more sensitive than linear; Fig. 10a; see also Sect. 3.2.6). This is primarily due to linear changes in the steady state temperature profile (Fig. 7a), though water velocities do increase slightly with higher temperatures (Fig. 7b), contribut-

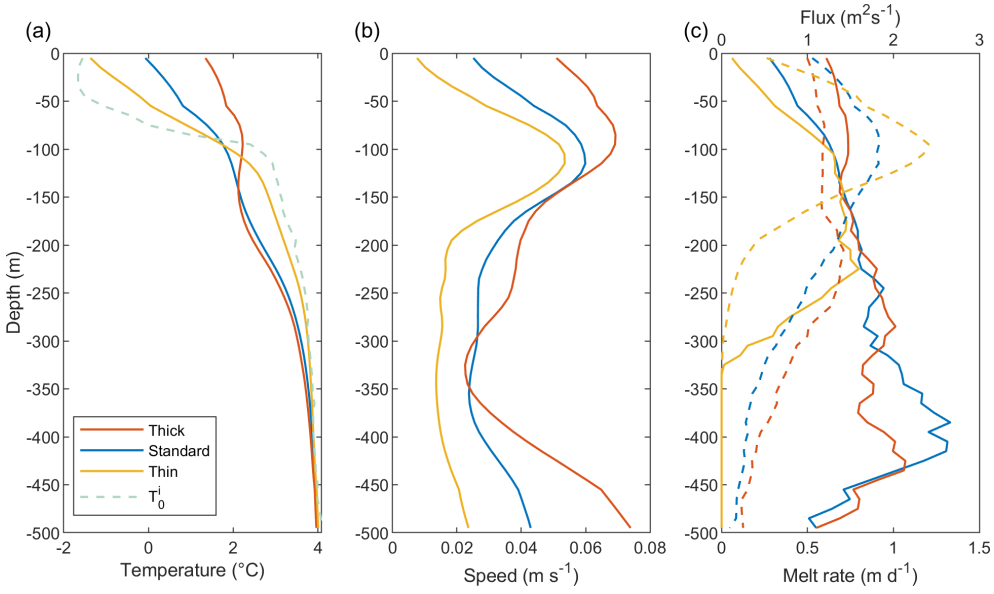

Figure 8. Sensitivity of ocean dynamics in the mélange to mélange thickness. **(a)** Temperature. The dashed line shows the imposed boundary condition. **(b)** Flow speed and **(c)** mélange melt rate (solid) and meltwater flux (dashed). All simulations have a subglacial discharge flux of $Q_0 = 300\,\mathrm{m^3\,s^{-1}}$, a temperature profile T_0 and an iceberg areal fraction $\lambda = 0.6$. All variables are averaged over the area of the mélange (the full width and depth of the fjord and 10 km down-fjord of the glacier terminus).

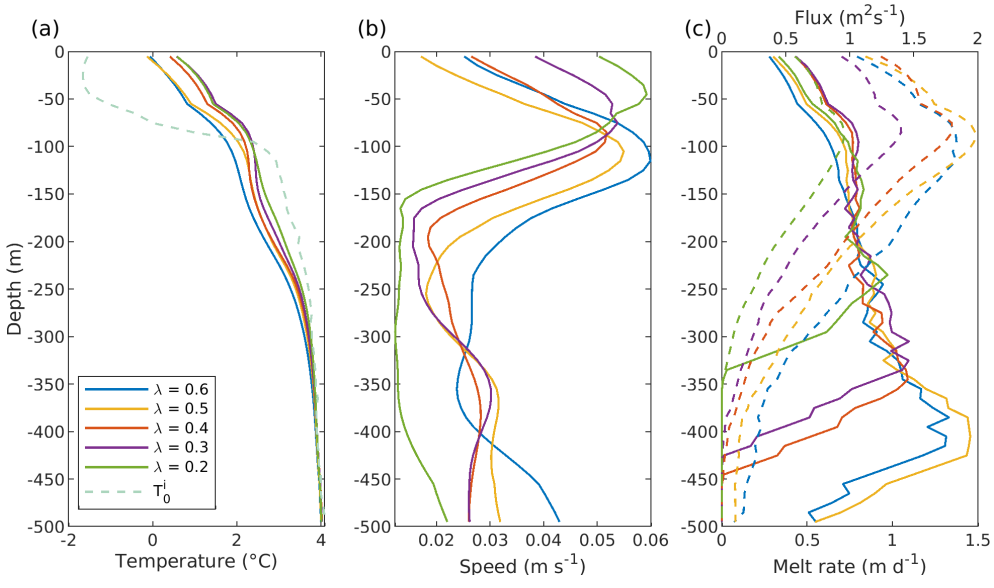

Figure 9. Sensitivity of ocean dynamics in the mélange to the iceberg areal fraction λ. **(a)** Temperature. The dashed line shows the imposed boundary condition. **(b)** Flow speed and **(c)** mélange melt rate (solid) and meltwater flux (dashed). All simulations have a subglacial discharge flux of $Q_0 = 300\,\mathrm{m^3\,s^{-1}}$, a temperature profile T_0 and a standard mélange thickness. All variables are averaged over the area of the mélange (the full width and depth of the fjord and 10 km down-fjord of the glacier terminus).

ing to increased melt rates. Mélange melt rates increase with mélange thickness in a non-linear fashion (Fig. 10a): whilst a thicker mélange generally results in a higher melt rate, this effect is less pronounced for higher values of subglacial discharge. This is because a higher subglacial discharge flux corresponds to a more vigorous plume which homogenises the temperature of the water column (Fig. 6a). As a result, thermal forcing is relatively uniform with depth and melt rates are similar for shallow- and deep-drafted icebergs for high values of subglacial discharge.

The sensitivity of the mélange melt rate to the iceberg areal fraction λ is complex. Melt rates generally increase with de-

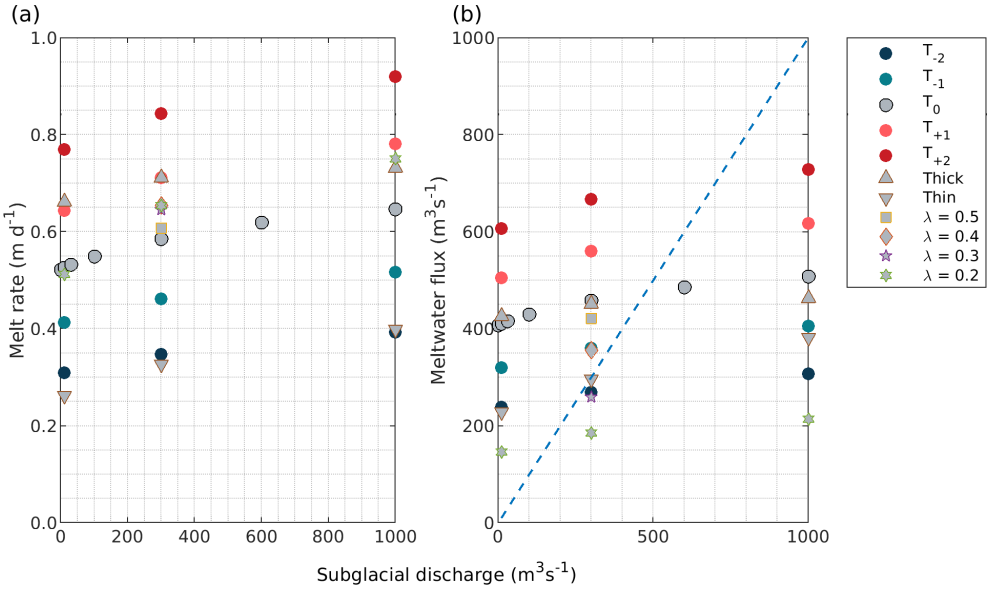

Figure 10. (a) The average melt rate and **(b)** total meltwater flux across all the simulations. The dashed blue line in **(b)** is the line for which the meltwater flux is equal to the subglacial discharge flux. The colour of the simulation refers to its boundary temperature profile, and the shape refers to its mélange thickness or iceberg areal fraction λ.

creasing λ, but below $\lambda = 0.4$ there is little senstivity of melt to λ (Fig. 10a). The sensitivity of mélange melt rate to subglacial discharge in the $\lambda = 0.2$ simulations is higher than that seen in the standard $\lambda = 0.6$ simulations.

The sensitivity of the total mélange meltwater flux to subglacial discharge and deep water temperature is similar to the sensitivity of the mean mélange melt rate to both of these variables (Fig. 10b). This is because the meltwater flux is simply the melt rate scaled by the mélange surface area. However, the thick mélange, which is comprised of a smaller total number of (larger) icebergs, has a smaller submerged surface area. This means that, despite the fact that the meltwater flux per unit area (i.e. the melt rate) for the thick mélange is higher than for the standard mélange (Fig. 10a), the total meltwater flux for the thick mélange is actually lower than the standard mélange meltwater flux (Fig. 10b). The reverse is true for the thin mélange, which is comprised of a larger total number of (smaller) icebergs and so has a larger submerged surface area. Relatively speaking, the total meltwater flux for the thin mélange is higher because of its large submerged surface area. With regards to the iceberg areal fraction λ, a lower value of λ decreases the total meltwater flux in an approximately linear fashion (Fig. 10b), since fewer icebergs generate less total meltwater.

3.2.6 Parameterisation

In light of the general trends discussed in Sect. 3.2.5 as well as previous studies which have parameterised submarine melting (e.g., Rignot et al., 2016), we seek a generalised parameterisation of the mélange melt rate m based on the simulations conducted in this study of the form

$$m = \left(a + bQ_0^c\right)\mathrm{TF}^d \tag{3}$$

where a, b, c, d are constants, Q_0 is the subglacial discharge, and TF represents the oceanic thermal forcing. The thermal forcing as a function of depth $\mathrm{TF}(z)$ is given by

$$\mathrm{TF}(z) = T(z) - T_\mathrm{f}(z) = T(z) - (\lambda_1 S(z) + \lambda_2 + \lambda_3 z) \tag{4}$$

where $T(z)$ and $S(z)$ are the restoring temperature and salinity profiles and the λ_i are constants used to calculate the in-situ freezing point $T_\mathrm{f}(z)$ (Jenkins, 2011). The thermal forcing which goes into the parameterisation of Eq. (3) is then the mean of $\mathrm{TF}(z)$ over a depth of 200–500 m, a choice we made since these are the source waters that are upwelling to provide most of the heat that melts the mélange. The thermal forcing is defined as a function of the forcing conditions $T(z)$ and $S(z)$ so that it can be calculated without the need to run any simulations.

On the whole, there is very solid agreement between simulated and parameterised melt rates (Fig. 11). The parameterisation is given in Eq. (3), with values of $a = 7.30 \times 10^{-2}$, $b = 4.12 \times 10^{-4}$, $c = 0.545$ and $d = 1.16$. The mean melt rates scale sublinearly with subglacial discharge (exponent 0.545) and slightly superlinearly with temperature (exponent 1.16). The value of $a = 0.073$ represents the background melting in the absence of any subglacial discharge, simply due to iceberg melting and the circulation which is set up as a result. Only the standard mélange thickness simulations with $\lambda = 0.6$ have been used to generate this parameterisation.

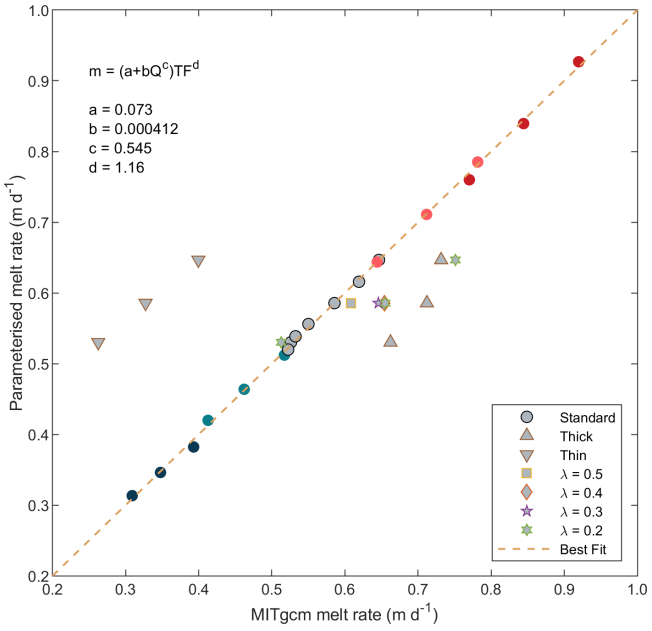

Figure 11. Parameterised melt rates compared with simulated melt rates. Simulations with standard mélange thickness are shown as circles; simulations with thick and thin mélange thickness are shown as upwards and downwards pointing triangles; other shapes refer to different values of the iceberg areal fraction λ. Only the standard mélange thickness simulations with $\lambda = 0.6$ are used to generate the parameterisation and best fit line. The temperature colour scheme is the same as Fig. 10.

4 Discussion

We have used MITgcm to model the circulation of ocean waters through a range of ice mélanges down-fjord from an idealised marine-terminating glacier system and estimate the resultant melt. The simulations suggest that warming always occurs in the top layer of the fjord, but that the magnitude of this warming grows with increased subglacial discharge, increased deep water temperature and increased mélange thickness. Similarly, water velocities increase – particularly in the upper 100 m of the fjord – with increased subglacial discharge, increased deep water temperature and increased mélange thickness. Since the simulated melt rate is a function of water temperature and velocity, and the meltwater flux is essentially the melt rate scaled by the mélange surface area, melt rates and meltwater flux also increase sublinearly with subglacial discharge, superlinearly with ocean temperature and non-linearly with mélange thickness. The melt rate dependence on subglacial discharge flux and ocean temperature can be summarised in a parameterisation with exponents of 0.55 and 1.16 respectively. Rignot et al. (2016) modelled the ocean melt of the calving front of multiple Greenlandic glaciers and obtained exponents of 0.39 and 1.18 for the sensitivities of the calving front melt rate on subglacial discharge and ocean temperature. This suggests that the ocean melt of ice mélange is broadly similar to the submarine melting of the calving front in terms of scalings with environmental forcings.

4.1 Limitations of the study

Uncertainty in the precise make-up of a mélange leads to uncertainty in the simulated melt rate. This uncertainty is primarily due to three factors: the mélange thickness, the distribution of icebergs in the mélange, and the iceberg areal fraction λ. Firstly, we have tried to create a realistic mélange by imposing a linearly decreasing mélange thickness. Our assumption that the mélange has a linearly decreasing profile is not unreasonable and is supported in some observational studies of mélange thickness, particularly in Sermilik Fjord (Enderlin et al., 2016). However, Burton et al. (2018) derive an exponentially-decreasing expression for mélange thickness which depends on the coefficient of internal friction of the mélange. A potential extension of the current study would be to investigate the effect of different mélange profile shapes on the simulated melt rate. In our simulations we see that melt rate decreases away from the terminus (Sect. 3.2.3; Fig. 8c) due to the imposed mélange profile. Therefore, if a mélange profile were to thin more quickly away from the terminus, we would expect melt rates to fall more quickly, decreasing the overall melt rate.

Secondly, we randomly sample icebergs from artificial iceberg distributions to create an ice mélange. Whilst observations look at the frequency of horizontal areas in an iceberg distribution pertaining to an entire ice mélange or fjord (Sulak et al., 2017; Shiggins et al., 2023), the method we have developed uses the frequency of iceberg drafts to generate five distinct iceberg distributions within the same ice mélange. This has the advantage of being able to generate a mélange with a realistic distribution of iceberg drafts as long as the mélange thickness is known or observed. However, this method assumes that it makes sense to have distinct iceberg distributions within the same mélange. We believe that, provided a given segment of the mélange is sufficiently large to have enough icebergs to describe a distribution, but sufficiently small that its mean iceberg draft is distinct from a separate segment, we would expect the iceberg populations of different segments of an ice mélange to be described by distinct power-law distributions. We chose to separate the mélange into five segments to attempt to achieve this balance between the segments having neither too many nor too few icebergs.

Thirdly, we stop randomly sampling icebergs once the iceberg areal fraction of the mélange reaches a specified value λ. For the majority of our simulations, including the one from which we develop the parameterisation, we set $\lambda = 0.6$, which represents a very densely packed ice mélange. There are very few observational estimates of λ, but those available suggest slightly lower values of $0.0 \leq \lambda \leq 0.4$ (Foga et al., 2014; Sulak et al., 2017). A lower value of λ increases

the simulated melt rate (Fig. 10a), as fewer icebergs in the mélange decreases the meltwater flux, reducing the cooling of the surface waters and thereby increasing the thermal forcing experienced by the mélange. However, this effect is only applicable up to a point, since the $\lambda = 0.2, 0.3, 0.4$ simulations all experience similar melt rates (Fig. 10a). The $\lambda = 0.2$ simulations are more sensitive to changes in subglacial discharge flux than the $\lambda = 0.6$ simulations (Fig. 10a). This suggests that a more advanced parameterisation of mélange melting could include a dependence on λ.

Iceberg shape is poorly represented in numerical models, which in turn leads to uncertainty in simulated melt rates. We have treated icebergs as smooth cuboids, which is clearly a simplification of the true range of iceberg shape and surface roughness. On the larger scale, cuboids resemble true icebergs with their steep and sharp vertical faces (Hughes, 2022), though large-scale roughness would have the potential to influence large-scale circulation. If cuboid icebergs were instead replaced with smooth cylinders, water would find different pathways through the mélange, impacting the overall flow and, as a result, the simulated melt rates. On the smaller scale, a rough ice surface may increase the turbulence of the water flow, producing ice scallops (Gilpin et al., 1980; Cenedese and Straneo, 2023). This can then further enhance the turbulent heat transfer to the ice, potentially increasing melt rates (Cenedese and Straneo, 2023). The impact of such surface details would have to be encapsulated in the melt rate parameterisation even in high-resolution studies.

Moreover, our iceberg geometries do not evolve throughout the simulation. Given maximum melt rates of approximately $0.9\,\mathrm{m\,d^{-1}}$ (Fig. 10a) and simulation run times of six days (Sect. 2.6), the change in iceberg geometry due to the melting over the course of a model run is less than the resolution of the model (20 m horizontal, 10 m vertical). As a result, we don't expect the lack of evolving iceberg geometries to have a significant impact on our results.

A key limitation in this study is the uncertainty associated with the exact form of the three-equation melt rate parameterisation which leads directly to uncertainty in the simulated mélange melt rates. In particular, whilst the standard form of this parameterisation uses a single value for the drag coefficient, in reality the drag experienced by fluid at the ice-ocean interface will depend both on the slope of the interface and the driver of the fluid flow itself. Zhao et al. (2024) found three specific flow regimes: plume-driven convection, melt-driven convection, and a general fjord-wide circulation. In light of this, we have tried to adapt the standard melt rate parameterisation (Holland and Jenkins, 1999; Jenkins, 2011) by using different values of the drag coefficient in different flow scenarios at the ice-ocean interface (Zhao et al., 2024). In particular, we have used thresholds on the fluid velocity in a particular grid cell as a mask for the three distinct melt regimes (Sect. 2.4). Despite this, converting a water velocity and temperature beside the ice to a generalised melt rate via a parameterisation is still limited by a lack of constraints on the values of parameters used in the parameterisation. More observational studies of iceberg melting are needed to decrease the uncertainty in these values.

In light of the above limitations, we have more confidence in the relative changes in mélange melt rate between different simulations than we do on the absolute values of melt rate found in this study. In other words, the sensitivity of the mélange melt rate to subglacial discharge flux, deep ocean temperature and mélange thickness found in this study are results which we believe are independent of the precise values of the constants used in the three-equation melt rate parameterisation. Furthermore, we also note that despite these potential limitations, our melt rate values are not dissimilar from those estimated in real ice mélange (Sect. 4.4).

4.2 Parameterisation

The parameterisation we have developed in Eq. (3) is limited by the lack of reference to the mélange thickness. The sensitivity of the simulation to mélange thickness was explored in Sect. 3.2.3. The influence of mélange thickness on modelled melt rates is complex: a thicker mélange leads to warmer near-surface waters (Fig. 8a) and higher velocities at all depths (Fig. 8b), but we were unable to find a simple way to include the mélange thickness in the melt rate parameterisation. The parameterisation overestimates the simulated melt rate in the thin simulations and underestimates the simulated melt rate in the thick simulations (Fig. 11): on average, the melt rate for the thin mélange is $0.26\,\mathrm{m\,d^{-1}}$ too high and the melt rate for the thick mélange is $0.11\,\mathrm{m\,d^{-1}}$ too low. We would expect the thickness to contribute to the thermal forcing term, with a thicker ice mélange experiencing higher thermal forcing due to an increased submerged surface area of ice in contact with deep warm water. Incorporating the mélange thickness into the parameterisation is a key task in future work.

4.3 Buttressing force

One of the key motivations for studying ice mélange is to understand the impact mélange melting may have on glacier dynamics. The mélange melt rate is a key control on mélange thickness, which in turn determines the buttressing force. Studies have shown that the buttressing force is highly sensitive to the submarine mélange melt rate (Amundson et al., 2025), meaning that an understanding of mélange melt rates is crucial to be able to accurately model the force balance at glacier termini. Our study provides an initial understanding of mélange melt rates which may in turn be used to understand the buttressing force provided by an ice mélange back onto a glacier. This may, in turn, be used to improve our understanding of the ocean forcing of the Greenland Ice Sheet. Building on the work done here, the next step would be to input a parameterised ice mélange melt rate into a model of

ice mélange dynamics (e.g. Amundson et al., 2025) to extract a buttressing force felt by the ice sheet.

Mélange thickness depends on the supply of icebergs into the mélange (i.e. the calving rate), the removal of icebergs from the mélange (i.e. the outflow into open fjord waters) and the melt rate of the mélange itself. Our results suggest that increased subglacial discharge and increased temperature of waters at depth in the fjord both result in higher mélange melt rates. Moreover, thicker mélange profiles, which extend deeper into warmer waters, experience significantly higher melt rates than thinner mélange profiles. An increase in the mélange melt rate will contribute to the mélange thinning over time, but the real relationship between melt rate and mélange thickness is complicated and depends on the iceberg flux into and out of the mélange. A potential extension of the current study would be to link mélange melt rates explicitly with calving rates at the glacier terminus via the buttressing force to gain a better understanding of the evolution of ice mélange. Observations of Sermeq Kujalleq by Joughin et al. (2020) suggest that the glacier responds to ocean forcing not through submarine melting of the glacier front but through the melting of its ice mélange and the associated variation in backstress. Our results here support the idea that the melting of an ice mélange would be sensitive to ocean temperature, and in particular to the deep ocean temperature within the fjord.

4.4 Comparison with observations

Our results are broadly comparable with observations of mélange melting. Across all simulations, the value for the mean mélange melt rate varies between 0.26–0.92 $\mathrm{m\,d^{-1}}$ and the total mélange meltwater flux varies between 186–729 $\mathrm{m^3\,s^{-1}}$. All observations discussed in this section studied Sermilik fjord, and so in theory should be directly comparable to our simulations.

Enderlin et al. (2016) use remote sensing at Sermilik fjord to find melt rates in the range of 0.05–0.67 $\mathrm{m\,d^{-1}}$ and meltwater fluxes in the range of 126–494 $\mathrm{m^3\,s^{-1}}$. They find that melt rates for deep-drafted icebergs are three times larger than melt rates for shallow icebergs, where they defined a deep-drafted (shallowed-drafted) iceberg as an iceberg whose draft is shallower (deeper) than the Polar-Atlantic Water Interface Depth. With respect to our standard simulation, the average melt rate at a depth of 50 m is approximately a third of the average melt rate at a depth of 400 m (Fig. 6c), which is comparable to the result from Enderlin et al. (2016). The observations from Enderlin et al. (2016) cover the months of June, July and October; their results likely cover a range of subglacial discharge fluxes and so it is sensible to compare to the full range of our results.

Moon et al. (2018) use observations at Sermilik fjord to drive an iceberg-melt model which includes melting via wave erosion, forced and free convection in air and (depth-dependent) forced and free convection in water, and estimate the mélange meltwater flux to be approximately 200–350 $\mathrm{m^3\,s^{-1}}$ in the summer assuming that the mélange constitutes 30 %–40 % of the total fjord iceberg melt. Moyer et al. (2019b) use Sentinel-2 imagery to analyse the region of Sermilik fjord outside of the ice mélange, but under the same assumption their estimate of the total meltwater flux between May and November is approximately 450–1460 $\mathrm{m^3\,s^{-1}}$.

Our simulations concur with the result found elsewhere that the iceberg meltwater flux is a dominant source of freshwater in the winter under low subglacial discharge scenarios (Enderlin et al., 2016; Moon et al., 2018). This is demonstrated clearly in Fig. 10b where the dashed line represents where the iceberg meltwater flux is equal to the subglacial discharge flux. For simulations above this line, the iceberg meltwater flux dominates; for simulations below this line, the subglacial discharge flux dominates. Our results suggest that for low subglacial discharges (i.e. winter) and higher ocean temperatures, iceberg meltwater flux is more likely to dominate; for higher subglacial discharges (i.e. summer) and lower ocean temperatures, the subglacial discharge flux is more likely to be the dominant freshwater source in a fjord system.

4.5 Comparison with similar studies

A number of other studies have simulated fjords with ice mélange. Hughes (2022) simulated the flow around hundreds of passive icebergs and found that the maximum average current speed was at or below the draft of the deepest icebergs. In our study, however, the maximum current speed was consistently around 100 m depth. There are three key differences in our model setup compared with that of Hughes (2022). Firstly, Hughes (2022) prescribes a half-sinusoid forcing velocity with zero depth mean, imposing a velocity at the surface and the seafloor to represent the overall velocity structure in many of Greenland's fjords. In contrast, we prescribe a boundary condition to explicitly represent subglacial discharge and observe the general velocity structure qualitatively (Figs. 3a, 6b, 7b, and 8b). Secondly, Hughes (2022) generates iceberg drafts explicitly from observed iceberg distributions such as Sulak et al. (2017), whereas we generate our own iceberg distributions as described in Sect. 2.3. Qualitatively, the iceberg distribution of our standard mélange is similar (compare our Fig. 2b to Fig. 3 in Hughes, 2022), but the percentage of deeper-drafted icebergs will be different for the different mélange profiles. Thirdly, we include thermodynamic effects, including melt-driven convection, which have an influence on the fjord-wide circulation which is established in the simulation. Taken together, we suggest that the depth of maximum current speed seems to be relatively insensitive to the maximum iceberg depths in the fjord and is instead mainly a function of the buoyancy of the plume and the strength of the subglacial discharge flux (Fig. 6b).

As discussed in Sect. 1, Davison et al. (2020) approximates iceberg melting by implementing the "IceBerg" pack-

age in MITgcm. This assigns an iceberg concentration to each grid box, estimates the resultant melting and then freshens, cools and accelerates the ocean water in each grid box accordingly. In contrast, we explicitly resolve the flow and melting around individual icebergs. Nevertheless, our results support the conclusions found in Davison et al. (2020) that the iceberg melt rate and meltwater flux scales with subglacial discharge and that iceberg melting is, on its own, a significant factor in the freshwater budget of a fjord and capable of driving its own fjord circulation.

4.6 Transferability to other systems

In terms of fjord dimensions, stratification and mélange thickness, our simulations have been designed to resemble Sermilik Fjord in southeast Greenland. We have tried to make our results more applicable to other systems by generalising the model setup and including different mélange thicknesses and temperature profiles. However, the overall shape of the temperature profile (in particular the temperature of the upper layer) is the same for all temperature anomalies, and all of our simulations have used a single salinity profile. Nevertheless, we expect our results to be applicable to systems that have similar characteristics to Sermilik fjord – that is, fjords of comparable dimensions with permanent ice mélange and a similar stratification of deep warm water underlying cooler water. We expect this to include other large glacier-fjord systems in Greenland, including Sermeq Kujalleq and Kangerlussuaq. The precise values in the melt rate parameterisation (Eq. 3) might vary, but the general concepts discussed above regarding the sensitivity of the mélange melt rate to subglacial discharge flux, deep ocean temperature and mélange thickness should carry over. In particular, we expect that the sensitivity to subglacial discharge flux will be sublinear (and so $c < 1$), and that the sensitivity to deep ocean temperature will be supralinear (and so $d > 1$). A potential extension of the current study would be to repeat the simulations with the specific geometry and oceanographic conditions of various glacier-fjord systems around Greenland.

5 Conclusions

The melting of an ice mélange can have a significant impact on a glacier and its fjord by reducing the buttressing force on a glacier terminus and releasing a substantial freshwater flux. Inspired by the need for a systematic analysis of how the ocean melt rate of ice mélange varies under different environmental conditions, we have run high-resolution numerical simulations using MITgcm to model the flow of waters through an ice mélange close to idealised marine-terminating glacier systems around Greenland and estimated the resultant melt. Specifically, we chose a domain size and ice mélange configuration based on the Helheim Glacier – Sermilik Fjord system, but our simulations are intended to be representative of large Greenlandic glacier-fjord systems.

We found that near-surface waters within the ice mélange always warm due to the upwelling of deep warm waters, driven both by the subglacial discharge plume and by the melt-driven convection on the sides of the icebergs themselves, and that the magnitude of this warming grows with increased subglacial discharge, increased deep water temperature and increased mélange thickness. Moreover, the magnitude of the simulated mélange melt rates varies from 0.26 to $0.92\,\mathrm{m\,d^{-1}}$ and is in good agreement with observational estimates.

Furthermore, we have developed a parameterisation of the mélange melt rate m which depends on the subglacial discharge flux Q_0 and the thermal forcing TF and is in the form $m = (a + bQ_0^c)\mathrm{TF}^d$, with $a = 7.30 \times 10^{-2}$, $b = 4.12 \times 10^{-4}$, $c = 0.545$ and $d = 1.16$. Our results highlight that mélange melt rates increase sublinearly with subglacial discharge and supralinearly with ocean temperature, suggesting that ocean melting of ice mélange follows similar environmental sensitivities as submarine melting at glacier calving fronts. The complex response of the melt rate to the thickness of an ice mélange meant that we were unable to incorporate the mélange thickness into this parameterisation, and doing so is a key task for future work. Nevertheless, this study is a step towards a better understanding of the sensitivity of mélange melting to changing environmental conditions – a crucial process to model accurately if we want to project how Greenland's glaciers and fjords will change in the future.

Appendix A: Generating an iceberg distribution

All modelled icebergs in this study are cuboid to simplify simulations, but in reality icebergs have infinitely many shapes. Nevertheless, assuming cuboid icebergs, there is a simple relationship between an iceberg's horizontal area A, total volume V and draft H: $V = AH \times (\rho_\mathrm{w}/\rho_\mathrm{i})$, where ρ_w and ρ_i are the densities of water and ice respectively. Since iceberg area is related to iceberg volume, and iceberg volume to iceberg draft for cuboid icebergs, in addition to the power law distribution $N \propto A^{-\alpha}$, we expect there to be a similar power law distribution of the form $N \propto H^{-\beta}$. That is, shallower icebergs should be much more common than deeper ones. Populating an artificial ice mélange by randomly sampling from an iceberg distribution of the form $N \propto H^{-\beta}$ is one way of respecting the fact that icebergs must replicate observed iceberg size power law distributions and have realistic aspect ratios as discussed in the main text.

Consider a power law distribution for the number of icebergs N of draft H of the form $N(H) = \eta H^{-\beta}$ with undetermined constants η and β. For this to be a probability distribution, we require $\int_{H_\mathrm{min}}^{H_\mathrm{max}} N(H) = 1$ where the parameters H_min and H_max represent the smallest and largest iceberg draft in the distribution. We set H_max to be the full

depth of the fjord – this represents the possibility of full-depth calving at the calving front. To determine $H_{\min}$, we combine $V = AH \times (\rho_w/\rho_i)$ and $V = aA^b$ to give an explicit relationship for iceberg draft H in terms of iceberg area A: $H = (\rho_i/\rho_w) \times aA^{b-1}$. There is a limit on the size of A determined by model resolution ($A_{\min} = dx \times dy$), and so $H_{\min}$ is set by $H_{\min} = (\rho_i/\rho_w) \times aA_{\min}^{b-1}$.

Applying the normalisation condition fixes the value of η and leaves only one undetermined constant β:

$$N(H) = \left(\frac{1-\beta}{H_{\max}^{1-\beta} - H_{\min}^{1-\beta}}\right) H^{-\beta} \tag{A1}$$

This is the same as Eq. (2) in the main text. The mean $\overline{N}$ of this distribution is then

$$\overline{N} = \frac{\int_{H_{\min}}^{H_{\max}} HN(H)dH}{\int_{H_{\min}}^{H_{\max}} N(H)dH} = \frac{1-\beta}{2-\beta} \times \frac{H_{\max}^{2-\beta} - H_{\min}^{2-\beta}}{H_{\max}^{1-\beta} - H_{\min}^{1-\beta}} \tag{A2}$$

$\overline{N} = \overline{N}(\beta, H_{\min}, H_{\max})$, i.e. $\overline{N}$ is a function of β, $H_{\min}$ and $H_{\max}$. $H_{\min}$ and $H_{\max}$ have been fixed above. $\overline{N}$ is set by observations of mean mélange thickness and then Eq. (A2) is used to determine β. In more detail: we split the domain into equal-width segments down-fjord, and pick a value mean mélange thickness $\overline{N}$ in each segment, based on observational data (e.g., Enderlin et al., 2016). We then numerically solve Eq. (A2) for β in each segment. This then provides a unique probability distribution of iceberg drafts $N(H)$ for each segment, with the mean of each probability distribution being the target mean draft of icebergs in that segment.

Appendix B: Inverse transform sampling

Inverse transform sampling is a way of randomly sampling from an arbitrary probability distribution. First, we make a cumulative distribution function $F(H)$ using the definition of $N(H)$ in Eq. (2):

$$F(H) = \int_{H_{\min}}^{H} N(t)dt = \frac{H^{1-\beta} - H_{\min}^{1-\beta}}{H_{\max}^{1-\beta} - H_{\min}^{1-\beta}} \tag{B1}$$

Next, we find the inverse $\tilde{F}(H)$:

$$\tilde{F}(H) = \left[H\left(H_{\max}^{1-\beta} - H_{\min}^{1-\beta}\right) + H_{\min}^{1-\beta}\right]^{\frac{1}{1-\beta}} \tag{B2}$$

To randomly sample an iceberg draft from our iceberg distribution, we generate a random number u such that $0 < u < 1$; a random iceberg draft h is then given by $h = \tilde{F}(u)$.

Appendix C: Table of simulations

Table C1. All the simulations run in this study. The naming convention is: mélange-thickness_subglacial-discharge-flux_temperature-profile_iceberg-areal-fraction, where "ms", "mk" and "mn" stand for a standard, thick and thin mélange thickness respectively and we only include the iceberg areal fraction in the name for $\lambda \neq 0.6$. The mélange geometry is given in terms of mean iceberg draft at the glacier terminus d_a and mean iceberg draft at the end of the mélange d_b.

Simulation name	Mélange geometry $[d_a, d_b]$ (m)	Q_0 ($m^3\ s^{-1}$)	Temperature profile	λ
ms_q0_t0	[100, 50]	0	T_0	0.6
ms_q10_t0	[100, 50]	10	T_0	0.6
ms_q30_t0	[100, 50]	30	T_0	0.6
ms_q100_t0	[100, 50]	100	T_0	0.6
ms_q300_t0	[100, 50]	300	T_0	0.6
ms_q600_t0	[100, 50]	600	T_0	0.6
ms_q1000_t0	[100, 50]	1000	T_0	0.6
ms_q10_t1	[100, 50]	10	T_1	0.6
ms_q300_t1	[100, 50]	300	T_1	0.6
ms_q1000_t1	[100, 50]	1000	T_1	0.6
ms_q10_t-1	[100, 50]	10	T_{-1}	0.6
ms_q300_t-1	[100, 50]	300	T_{-1}	0.6
ms_q1000_t-1	[100, 50]	1000	T_{-1}	0.6
ms_q10_t2	[100, 50]	10	T_2	0.6
ms_q300_t2	[100, 50]	300	T_2	0.6
ms_q1000_t2	[100, 50]	1000	T_2	0.6
ms_q10_t-2	[100, 50]	10	T_{-2}	0.6
ms_q300_t-2	[100, 50]	300	T_{-2}	0.6
ms_q1000_t-2	[100, 50]	1000	T_{-2}	0.6
mk_q10_t0	[200, 100]	10	T_0	0.6
mk_q300_t0	[200, 100]	300	T_0	0.6
mk_q1000_t0	[200, 100]	1000	T_0	0.6
mn_q10_t0	[50, 25]	10	T_0	0.6
mn_q300_t0	[50, 25]	300	T_0	0.6
mn_q1000_t0	[50, 25]	1000	T_0	0.6
ms_q300_t0_l5	[100, 50]	300	T_0	0.5
ms_q300_t0_l4	[100, 50]	300	T_0	0.4
ms_q300_t0_l3	[100, 50]	300	T_0	0.3
ms_q10_t0_l2	[100, 50]	10	T_0	0.2
ms_q300_t0_l2	[100, 50]	300	T_0	0.2
ms_q1000_t0_l2	[100, 50]	1000	T_0	0.2

Code availability. The archive accessible at https://doi.org/10.5281/zenodo.15577774 (Jain, 2025) includes the code needed to generate the ice mélange profiles, the code needed to run the MITgcm simulations, and the output of the last timestep of the ms_q300_t0 simulation.

Data availability. The CTD profiles used are available at https://doi.org/10.18739/A2M03XZ2K (Straneo, 2021).

Author contributions. LJ, DAS and PN designed the research. LJ set up the MITgcm runs with help from DAS. LJ ran the simulations and analysed the results. LJ wrote the paper, with input from all other authors.

Competing interests. The contact author has declared that none of the authors has any competing interests.

Disclaimer. Publisher's note: Copernicus Publications remains neutral with regard to jurisdictional claims made in the text, published maps, institutional affiliations, or any other geographical representation in this paper. While Copernicus Publications makes ev-

ery effort to include appropriate place names, the final responsibility lies with the authors. Views expressed in the text are those of the authors and do not necessarily reflect the views of the publisher.

Acknowledgements. LJ is funded by NERC through the E4 DTP studentship NE/S007407/1. DAS acknowledges support from NERC Independent Research Fellowship NE/T011920/1. The authors would also like to thank Erwin Lambert and Ellyn Enderlin for reviewing this paper and providing very helpful comments, corrections and suggestions which improved several aspects of the text.

Financial support. This research has been supported by the Natural Environment Research Council (grant nos. NE/S007407/1 and NE/T011920/1).

Review statement. This paper was edited by Kerim Nisancioglu and reviewed by Erwin Lambert and Ellyn Enderlin.

References

Amundson, J. M., Fahnestock, M., Truffer, M., Brown, J., Lüthi, M. P., and Motyka, R. J.: Ice mélange dynamics and implications for terminus stability, Jakobshavn Isbræ, Greenland, Journal of Geophysical Research: Earth Surface, 115, https://doi.org/10.1029/2009JF001405, 2010.

Amundson, J. M., Robel, A. A., Burton, J. C., and Nissanka, K.: A quasi-one-dimensional ice mélange flow model based on continuum descriptions of granular materials, The Cryosphere, 19, 19–35, https://doi.org/10.5194/tc-19-19-2025, 2025.

Åström, J., Cook, S., Enderlin, E. M., Sutherland, D. A., Mazur, A., and Glasser, N.: Fragmentation theory reveals processes controlling iceberg size distributions, Journal of Glaciology, 67, 603–612, https://doi.org/10.1017/jog.2021.14, 2021.

Bevan, S. L., Luckman, A. J., Benn, D. I., Cowton, T., and Todd, J.: Impact of warming shelf waters on ice mélange and terminus retreat at a large SE Greenland glacier, The Cryosphere, 13, 2303–2315, https://doi.org/10.5194/tc-13-2303-2019, 2019.

Burton, J. C., Amundson, J. M., Cassotto, R., Kuo, C.-C., and Dennin, M.: Quantifying flow and stress in ice mélange, the world's largest granular material, Proceedings of the National Academy of Sciences, 115, 5105–5110, https://doi.org/10.1073/pnas.1715136115, 2018.

Carroll, D., Sutherland, D. A., Shroyer, E. L., Nash, J. D., Catania, G. A., and Stearns, L. A.: Modeling Turbulent Subglacial Meltwater Plumes: Implications for Fjord-Scale Buoyancy-Driven Circulation, Journal of Physical Oceanography, 45, 2169–2185, https://doi.org/10.1175/JPO-D-15-0033.1, 2015.

Catania, G. A., Stearns, L. A., Sutherland, D. A., Fried, M. J., Bartholomaus, T. C., Morlighem, M., Shroyer, E., and Nash, J.: Geometric Controls on Tidewater Glacier Retreat in Central Western Greenland, Journal of Geophysical Research: Earth Surface, 123, 2024–2038, https://doi.org/10.1029/2017JF004499, 2018.

Cenedese, C. and Straneo, F.: Icebergs Melting, Annual Review of Fluid Mechanics, 55, 377–402, https://doi.org/10.1146/annurev-fluid-032522-100734, 2023.

Cowton, T., Slater, D., Sole, A., Goldberg, D., and Nienow, P.: Modeling the impact of glacial runoff on fjord circulation and submarine melt rate using a new subgrid-scale parameterization for glacial plumes, Journal of Geophysical Research: Oceans, 120, 796–812, https://doi.org/10.1002/2014JC010324, 2015.

Cowton, T., Sole, A., Nienow, P., Slater, D., Wilton, D., and Hanna, E.: Controls on the transport of oceanic heat to Kangerdlugssuaq Glacier, East Greenland, Journal of Glaciology, 62, https://doi.org/10.1017/jog.2016.117, 2016.

Davison, B. J., Cowton, T. R., Cottier, F. R., and Sole, A. J.: Iceberg melting substantially modifies oceanic heat flux towards a major Greenlandic tidewater glacier, Nature Communications, 11, 5983, https://doi.org/10.1038/s41467-020-19805-7, 2020.

Davison, B. J., Cowton, T., Sole, A., Cottier, F., and Nienow, P.: Modelling the effect of submarine iceberg melting on glacier-adjacent water properties, The Cryosphere, 16, 1181–1196, https://doi.org/10.5194/tc-16-1181-2022, 2022.

Enderlin, E. M., Hamilton, G. S., Straneo, F., and Sutherland, D. A.: Iceberg meltwater fluxes dominate the freshwater budget in Greenland's iceberg-congested glacial fjords, Geophysical Research Letters, 43, 11287–11294, https://doi.org/10.1002/2016GL070718, 2016.

FitzMaurice, A., Cenedese, C., and Straneo, F.: Nonlinear response of iceberg side melting to ocean currents, Geophysical Research Letters, 44, 5637–5644, https://doi.org/10.1002/2017GL073585, 2017.

Foga, S., Stearns, L. A., and van der Veen, C.: Application of Satellite Remote Sensing Techniques to Quantify Terminus and Ice Mélange Behavior at Helheim Glacier, East Greenland, Marine Technology Society Journal, 48, 81–91, https://doi.org/10.4031/MTSJ.48.5.3, 2014.

Gilpin, R. R., Hirata, T., and Cheng, K. C.: Wave formation and heat transfer at an ice-water interface in the presence of a turbulent flow, Journal of Fluid Mechanics, 99, 619–640, https://doi.org/10.1017/S0022112080000791, 1980.

Hester, E. W., McConnochie, C. D., Cenedese, C., Couston, L.-A., and Vasil, G.: Aspect ratio affects iceberg melting, Physical Review Fluids, 6, 023802, https://doi.org/10.1103/PhysRevFluids.6.023802, 2021.

Holland, D. M. and Jenkins, A.: Modeling Thermodynamic Ice–Ocean Interactions at the Base of an Ice Shelf, Journal of Physical Oceanography, 29, 1787–1800, https://doi.org/10.1175/1520-0485(1999)029<1787:MTIOIA>2.0.CO;2, 1999.

Howat, I. M., Joughin, I., Tulaczyk, S., and Gogineni, S.: Rapid retreat and acceleration of Helheim Glacier, east Greenland, Geophysical Research Letters, 32, https://doi.org/10.1029/2005GL024737, 2005.

Howat, I. M., Box, J. E., Ahn, Y., Herrington, A., and McFadden, E. M.: Seasonal variability in the dynamics of marine-terminating outlet glaciers in Greenland, Journal of Glaciology, 56, 601–613, https://doi.org/10.3189/002214310793146232, 2010.

Hughes, K. G.: Pathways, Form Drag, and Turbulence in Simulations of an Ocean Flowing Through an Ice Mélange, Journal of Geophysical Research: Oceans, 127, e2021JC018228, https://doi.org/10.1029/2021JC018228, 2022.

Hughes, K. G.: Fjord circulation induced by melting icebergs, The Cryosphere, 18, 1315–1332, https://doi.org/10.5194/tc-18-1315-2024, 2024.

Jackson, R. H., Nash, J. D., Kienholz, C., Sutherland, D. A., Amundson, J. M., Motyka, R. J., Winters, D., Skyllingstad, E., and Pettit, E. C.: Meltwater Intrusions Reveal Mechanisms for Rapid Submarine Melt at a Tidewater Glacier, Geophysical Research Letters, 47, e2019GL085335, https://doi.org/10.1029/2019GL085335, 2020.

Jain, L.: Modelling ocean melt of ice mélange at Greenland's marine-terminating glaciers: datasets and code, Zenodo [code], https://doi.org/10.5281/zenodo.15577774, 2025.

Jenkins, A.: Convection-Driven Melting near the Grounding Lines of Ice Shelves and Tidewater Glaciers, Journal of Physical Oceanography, 41, 2279–2294, https://doi.org/10.1175/JPO-D-11-03.1, 2011.

Jenkins, A., Dutrieux, P., Jacobs, S. S., McPhail, S. D., Perrett, J. R., Webb, A. T., and White, D.: Observations beneath Pine Island Glacier in West Antarctica and implications for its retreat, Nature Geoscience, 3, 468–472, https://doi.org/10.1038/ngeo890, 2010.

Joughin, I., Smith, B. E., Howat, I. M., Floricioiu, D., Alley, R. B., Truffer, M., and Fahnestock, M.: Seasonal to decadal scale variations in the surface velocity of Jakobshavn Isbrae, Greenland: Observation and model-based analysis, Journal of Geophysical Research: Earth Surface, 117, https://doi.org/10.1029/2011JF002110, 2012.

Joughin, I., Shean, D. E., Smith, B. E., and Floricioiu, D.: A decade of variability on Jakobshavn Isbræ: ocean temperatures pace speed through influence on mélange rigidity , The Cryosphere, 14, 211–227, https://doi.org/10.5194/tc-14-211-2020, 2020.

Kajanto, K., Straneo, F., and Nisancioglu, K.: Impact of icebergs on the seasonal submarine melt of Sermeq Kujalleq, The Cryosphere, 17, 371–390, https://doi.org/10.5194/tc-17-371-2023, 2023.

Karlsson, N. B., Mankoff, K. D., Solgaard, A. M., Larsen, S. H., How, P. R., Fausto, R. S., and Sørensen, L. S.: A data set of monthly freshwater fluxes from the Greenland ice sheet's marine-terminating glaciers on a glacier–basin scale 2010–2020, GEUS Bulletin, 53, https://doi.org/10.34194/geusb.v53.8338, 2023.

King, M. D., Howat, I. M., Candela, S. G., Noh, M. J., Jeong, S., Noël, B. P. Y., van den Broeke, M. R., Wouters, B., and Negrete, A.: Dynamic ice loss from the Greenland Ice Sheet driven by sustained glacier retreat, Communications Earth & Environment, 1, 1–7, https://doi.org/10.1038/s43247-020-0001-2, 2020.

Krug, J., Durand, G., Gagliardini, O., and Weiss, J.: Modelling the impact of submarine frontal melting and ice mélange on glacier dynamics, The Cryosphere, 9, 989–1003, https://doi.org/10.5194/tc-9-989-2015, 2015.

Losch, M.: Modeling ice shelf cavities in a z coordinate ocean general circulation model, Journal of Geophysical Research: Oceans, 113, https://doi.org/10.1029/2007JC004368, 2008.

Mankoff, K. D., Noël, B., Fettweis, X., Ahlstrøm, A. P., Colgan, W., Kondo, K., Langley, K., Sugiyama, S., van As, D., and Fausto, R. S.: Greenland liquid water discharge from 1958 through 2019, Earth Syst. Sci. Data, 12, 2811–2841, https://doi.org/10.5194/essd-12-2811-2020, 2020.

Marshall, J., Adcroft, A., Hill, C., Perelman, L., and Heisey, C.: A finite-volume, incompressible Navier Stokes model for studies of the ocean on parallel computers, Journal of Geophysical Research: Oceans, 102, 5753–5766, https://doi.org/10.1029/96JC02775, 1997a.

Marshall, J., Hill, C., Perelman, L., and Adcroft, A.: Hydrostatic, quasi-hydrostatic, and nonhydrostatic ocean modeling, Journal of Geophysical Research: Oceans, 102, 5733–5752, https://doi.org/10.1029/96JC02776, 1997b.

Meng, Y., Lai, C. Y., Culberg, R., Shahin, M. G., Stearns, L. A., Burton, J. C., and Nissanka, K.: Seasonal changes of mélange thickness coincide with Greenland calving dynamics. Nat Commun 16, 573, https://doi.org/10.1038/s41467-024-55241-7, 2025.

Moon, T., Sutherland, D. A., Carroll, D., Felikson, D., Kehrl, L., and Straneo, F.: Subsurface iceberg melt key to Greenland fjord freshwater budget, Nature Geoscience, 11, 49–54, https://doi.org/10.1038/s41561-017-0018-z, 2018.

Moyer, A. N., Nienow, P. W., Gourmelen, N., Sole, A. J., and Slater, D. A.: Estimating Spring Terminus Submarine Melt Rates at a Greenlandic Tidewater Glacier Using Satellite Imagery, Frontiers in Earth Science, 5, https://doi.org/10.3389/feart.2017.00107, 2017.

Moyer, A. N., Nienow, P. W., Gourmelen, N., Sole, A. J., Slater, D. A., Truffer, M., and Fahnestock, M.: Spatio-temporal variations in seasonal ice tongue submarine melt rate at a tidewater glacier in southwest Greenland, Journal of Glaciology, 65, 523–530, https://doi.org/10.1017/jog.2019.27, 2019a.

Moyer, A. N., Sutherland, D. A., Nienow, P. W., and Sole, A. J.: Seasonal Variations in Iceberg Freshwater Flux in Sermilik Fjord, Southeast Greenland From Sentinel-2 Imagery, Geophysical Research Letters, 46, 8903–8912, https://doi.org/10.1029/2019GL082309, 2019b.

O'Leary, M. and Christoffersen, P.: Calving on tidewater glaciers amplified by submarine frontal melting, The Cryosphere, 7, 119–128, https://doi.org/10.5194/tc-7-119-2013, 2013.

Rignot, E., Xu, Y., Menemenlis, D., Mouginot, J., Scheuchl, B., Li, X., Morlighem, M., Seroussi, H., den Broeke, M. v., Fenty, I., Cai, C., An, L., and Fleurian, B. d.: Modeling of ocean-induced ice melt rates of five west Greenland glaciers over the past two decades, Geophysical Research Letters, 43, 6374–6382, https://doi.org/10.1002/2016GL068784, 2016.

Robel, A. A.: Thinning sea ice weakens buttressing force of iceberg mélange and promotes calving, Nature Communications, 8, 14596, https://doi.org/10.1038/ncomms14596, 2017.

Shiggins, C. J., Lea, J. M., and Brough, S.: Automated ArcticDEM iceberg detection tool: insights into area and volume distributions, and their potential application to satellite imagery and modelling of glacier–iceberg–ocean systems, The Cryosphere, 17, 15–32, https://doi.org/10.5194/tc-17-15-2023, 2023.

Slater, D. A. and Straneo, F.: Submarine melting of glaciers in Greenland amplified by atmospheric warming, Nature Geoscience, 15, 794–799, https://doi.org/10.1038/s41561-022-01035-9, 2022.

Straneo, F.: Profiles of temperature and salinity from Sermilik Fjord during March 2010, Arctic Data Center [data set], https://doi.org/10.18739/A2M03XZ2K, 2021.

Straneo, F. and Heimbach, P.: North Atlantic warming and the retreat of Greenland's outlet glaciers, Nature, 504, 36–43, https://doi.org/10.1038/nature12854, 2013.

Straneo, F., Curry, R. G., Sutherland, D. A., Hamilton, G. S., Cenedese, C., Våge, K., and Stearns, L. A.: Im-

pact of fjord dynamics and glacial runoff on the circulation near Helheim Glacier, Nature Geoscience, 4, 322–327, https://doi.org/10.1038/ngeo1109, 2011.

Straneo, F., Hamilton, G. S., Stearns, L. A., and Sutherland, D. A.: Connecting the Greenland Ice Sheet and the Ocean: A Case Study of Helheim Glacier and Sermilik Fjord, Oceanography, 29, 34–45, 2016.

Sulak, D. J., Sutherland, D. A., Enderlin, E. M., Stearns, L. A., and Hamilton, G. S.: Iceberg properties and distributions in three Greenlandic fjords using satellite imagery, Annals of Glaciology, 58, 92–106, https://doi.org/10.1017/aog.2017.5, 2017.

Sutherland, D. A., Jackson, R. H., Kienholz, C., Amundson, J. M., Dryer, W. P., Duncan, D., Eidam, E. F., Motyka, R. J., and Nash, J. D.: Direct observations of submarine melt and subsurface geometry at a tidewater glacier, Science, 365, 369–374, https://doi.org/10.1126/science.aax3528, 2019.

The IMBIE Team: Mass balance of the Greenland Ice Sheet from 1992 to 2018, Nature, 579, 233–239, https://doi.org/10.1038/s41586-019-1855-2, 2020.

Wehrlé, A., Lüthi, M. P., and Vieli, A.: The control of short-term ice mélange weakening episodes on calving activity at major Greenland outlet glaciers, The Cryosphere, 17, 309–326, https://doi.org/10.5194/tc-17-309-2023, 2023.

Wood, M., Rignot, E., Fenty, I., An, L., Bjørk, A., van den Broeke, M., Cai, C., Kane, E., Menemenlis, D., Millan, R., Morlighem, M., Mouginot, J., Noël, B., Scheuchl, B., Velicogna, I., Willis, J. K., and Zhang, H.: Ocean forcing drives glacier retreat in Greenland, Science Advances, 7, eaba7282, https://doi.org/10.1126/sciadv.aba7282, 2021.

Xu, Y., Rignot, E., Menemenlis, D., and Koppes, M.: Numerical experiments on subaqueous melting of Greenland tidewater glaciers in response to ocean warming and enhanced subglacial discharge, Annals of Glaciology, 53, 229–234, https://doi.org/10.3189/2012AoG60A139, 2012.

Zhao, K. X., Skyllingstad, E. D., and Nash, J. D.: Improved Parameterizations of Vertical Ice-Ocean Boundary Layers and Melt Rates, Geophysical Research Letters, 51, e2023GL105862, https://doi.org/10.1029/2023GL105862, 2024.